# Function of Cerebellar Microcircuitry within a Closed-loop System during Control and Adaptation

Anton Spanne

| Lund University<br>**Department of Automatic Control**<br>**Box 118**<br>**SE-221 00 Lund Sweden** | *Document name*<br>MASTER THESIS |
|---|---|
| | *Date of issue*<br>April 2011 |
| | *Document Number*<br>ISRN LUTFD2//TFRT--5877--SE |
| *Author(s)*<br>Anton Spanne | *Supervisor*<br>Henrik Jörntell NRC, Lund University, Sweden<br>Rolf Johansson Automatic Control Lund, Sweden<br>(Examiner) |
| | *Sponsoring organization* |

*Title and subtitle*

Function of Cerebellar Microcircuitry within a Closed-loop System during Control and Adaptation
(Egenskaper hos lillhjärnan som en krets inom ett återkopplat system vid adaptation och reglering)

*Abstract*

The human motor control is both robust and stable, despite large delays and highly complex motor systems with an abundance of actuators, sensors and degrees of freedom. The cerebellum is thought help accomplish this by compensating for external loads and internal limitations and disturbances through adaptation, creating inverse models of the motor system dynamics. The cerebellum does also exhibit a generic relatively well described modular microcircuitry, making it a suitable neural circuitry to study.

This thesis models a small part of the cerebellum, using detailed bio-physical models in combination with rate-based models, and uses the constructed network model to improve control of a planar double joint arm.The individual neuron models were calibrated using data from in vivo experiments. The response from the models when they were introduced to recorded primary afferent spike trains, originating from tactile stimulation, was used to validate their behaviour. Subsets of the complete network was also constructed to investigate possible functions of the granule cells and inhibitory connection patterns between interneurons within the molecular layer.

*Keywords*

*Classification system and/or index terms (if any)*

*Supplementary bibliographical information*

http://www.control.lth.se/publications/

# Sammanfattning

Egenskaper hos lillhjärnan som en krets inom ett återkopplat system vid adaptation och reglering

Människans motoriska reglersystem är både robust och stabilt, trots långa fördröjningar och en hög komplexitet hos det motoriska systemet, med ett överflöd av ställdon, givare och frihetsgrader. Det verkar som lillhjärnan hjälper till att åstadkomma detta genom att kompensera för yttre belastningar och inre störningar genom att skapa en invers modell av the styrda systemet. Lillhjärnan uppvisar också en generell och relativt välbeskriven nätverksstruktur, vilket gör det än mer passande att studera den. I den här studien modelleras en liten del av lillhjärnan med bio-fysikaliskt detaljerade nervcellsmodeller i kombination med escape-rate-modeller, och använder det konstruerade nätverket för att reglera en två-ledad arm i ett plan. De enskilda nervcellsmodellerna kalibreras med hjälp av data från in-vivo försök. Deras beteende när de utsätts för spiktåg från primärafferenter, under tiden dessa blev mekaniskt stimulerade, används för att validera modellerna. Mindre delar av nätverket används också för att undersöka möjliga funktioner hos det granulära lagret och hos återkopplade inhibitoriska kopplingsmönster mellan interneuroner i det molekylära lagret

# Nomenclature

# Contents

# 1. Introduction

## 1.1 Background

The cerebellum is a structure of the brain that resides beneath and separate from the cerebral hemispheres. Since the beginning of the 19th century, it has been known to play a crucial role in movement control, preventing end point oscillations and increasing coordination, precision and timing. This was based upon cases of cerebellar lesions, where it could be shown that it was the coordination of movements rather than their strength that was affected by the lesion [Manto, 2008].

By current knowledge, the cerebellum is involved in motion control and learning, but is not responsible for initiating movement. However, even though the cerebellar anatomy is to large extent known and gives evidence of a highly regular structure, the details of the cerebellar functionality is still debated.

The anatomical structure of the cerebellum, with a small amount of Purkinje cells receiving input from a large set of sensory and motor command sources, has lead to the hypothesis that the cerebellum works as an adaptive filter. In accordance with this, individual synaptic weights has been observed to change in correlation with proposed error signals from climbing fibers through Long Term Depression (LTD) and Long Term Potentiation (LTP) [Jörntell and Ekerot, 2002].

From a control theory perspective it has been proposed that the trained cerebellum mimics the forward or/and inverse dynamics of the plant that it is controlling. The forward dynamics can be used similar to a Smith predictor, cancelling some of the error due to slow feedback, while the inverse dynamics can work as a feed forward controller. More advanced proposed abstract models of the cerebellar functionality include both the inverse and forward dynamics, in order to build cascaded linear controllers used during different circumstances, such as different arm positions or loads [Kawato, 1999].

Analysing the cerebellum and the abundance of biological sensors and actuators it uses for control can yield interesting perspectives into how highly adaptive systems can be built and how deficient sensory information can be used. The system also suffers from its, in comparison with modern control systems, slow feedback and muscle response times, giving rise to another set of classical control problems that is somehow solved within the cerebellar control loop.

By building and using a biologically plausible simulation toolbox, different features of the cerebellar microcircuitry can be explored. Such a tool could also be used to analyze the simultaneous behaviour of larger sets of neurons than possible during *in vivo/vitro* studies. Currently, even though the anatomical structure of the cerebellum is known, the behaviour of several neurons in concert is not as well studied.

## 1.2 Thesis outline

This thesis work can be divided into two consecutive steps. First, suitable models for all neuron types have to be selected based on the characteristics of the neurons. These models then have to be fitted to known data and validated through simulation, comparing the result to real measurements.

Secondly, two cerebellar microzones should be modelled using the neuron models, connecting the networks output and input according to the experimental setup in [Schweighofer *et al.*, 1998, I]. The microzones should be responsible for controlling one joint each in the double joint arm, and the number of neurons in each microzone should be determined by simulation speed requirements, but still be large enough to give valid simulation results.

The aim of the work is to create a working simulation environment for the cerebellum, with models of the major neuron types. This can then be used to further investigate the behaviour and limitations of the cerebellar network and the simulation results can be used to validate or discredit existing hypotheses.

## 1.3   Method overview

The entire simulation environment is written in the Java language[1], using its built in multi-threading capabilities. Because of the relatively long delays of neural networks and the signaling system between individual neurons, the system is ideal for asynchronous simulation. A simple syntax that feeds the network structure to the simulation environment is also defined and used to create different experimental setups. Most of the resulting data generated from the simulations are manipulated and put into graphs using Matlab[2].

Suitable neuron models are chosen to each of the neurons types using *in vivo* data, taking their proposed role within the network into consideration. The neurons that are modelled with stochastic spike generation uses some of the results from [Dürango, 2010] to choose suitable ISI distributions. An extended model of bursting neurons building upon the work in [Smith *et al.*, 2000] is used to simulate the bursting behaviour of neurons in the cunate nucleus. All the models are validated against *in vivo* measurements at the different layers of the network with standardized afferent tactile and current pulse stimuli.

In order to evaluate the performance of an entire network, the setup from [Schweighofer *et al.*, 1998, II] is used, where the cerebellum model is adapted into an inverse model of a double joint arm. The network is used to improve the performance of a slow feedback and linear feed-forward controller that acts in parallel to the network on the arm. The synaptic weight update rules from [Schweighofer *et al.*, 1996] are used to train the model, using a multi-modal error signal containing the position, speed and acceleration error.

All experimental data used in the work is *in vivo* recordings from the cat cerebellum, provided by Henrik Jörntell at the Department of Experimental Medical Sciences, Section for Neurophysiology, Lund University.

---

[1]http://www.java.com/

[2]http://www.mathworks.com/products/matlab/

# 2. Spiking neuron models

The foundation of information processing in all biological nervous systems relies on the electrical properties of the neuron. It reacts to synaptic inputs from other neurons, transmitted through specialized ion-channels in the cell membrane. The information is sent between the neurons as depolarized potential spikes or action potentials, which activates ion-channels at the synapses connecting the neuron to subsequent neurons. In turn, the ion-channels cause depolarization of the membrane potential if the synapse is excitatory, or hyperpolarization if it is inhibitory. Enough excitatory input will cause the subsequent neuron to generate an action potential of its own, sending the information further down through the network.

The basic structure of simulated neural networks make few assumptions regarding the functions of the individual neurons and how they communicate. The least detailed neuron model, the perceptron, which is used extensively in artificial neural networks, works as a simple binary classifier. To determine whether it is active or not, all inputs are summed, and the perceptron is activated if the sum reaches a given threshold. The binary state of each perceptron, and the fact that the network has no memory or time dependencies, makes them suitable for classification tasks and to study fundamental properties of neural networks [Widrow and Walach, 2007].

In the other range of the spectrum, a neuron can also be modeled in detail, taking many of the its bio-physical aspects into consideration. The Hodgkin-Huxley model, first presented in [Hodgkin and Huxley, 1952], uses several internal states to model the non-linear membrane potential dependant behaviour of the different ion-channels populating the neuron cell membrane. The complete model can be seen in Eq. (2.1), where the membrane current is described by a leak current and two ion-channels, whose conductivity depends on the three states $m$, $n$ and $h$. The model can also be extended to support additional types of ion channels, other than the sodium and potassium channels shown in Eq. (2.1).

$$
\begin{aligned}
C_m \frac{dV_m}{dt} &= -I_{ion} + I_{ext} \\
I_{ion} &= \bar{g}_{Na} m^3 h \left( V_m - E_{Na} \right) + \bar{g}_K n^4 \left( V_m - E_K \right) + \bar{g}_L \left( V_m - E_L \right) \\
\frac{m}{dt} &= \alpha_m \left( V \right) \left( 1 - m \right) - \beta_m \left( V \right) m \\
\frac{h}{dt} &= \alpha_h \left( V \right) \left( 1 - h \right) - \beta_h \left( V \right) h \\
\frac{n}{dt} &= \alpha_n \left( V \right) \left( 1 - n \right) - \beta_n \left( V \right) n
\end{aligned}
\tag{2.1}
$$

Even though the Hodgkin-Huxley model manages to emulate the membrane potential of a single neuron in great detail, including the formation of action potentials, it includes no description of how the neurons interact. Under the common assumption that the shape of the action potential has no influence over the behaviour of the activated synapses, an action potential can be viewed as a discrete event, fully described by the time it was generated. Furthermore, if the information carried by the axons can be fully described by the spiking intensity, the intensity or spike rate could be used in the network model instead of actual spikes to carry the information between connected neurons.

As the intensity is the average firing rate, it requires the introduction of a artificial time constant governing the length of the averaging interval. This time constant im-

poses restrictions to the signal that would not be needed if the actual spike times were used to transmit the information. Using the spike times, the first spike of a spike train is transmitted immediately, while the time constant used to calculate the intensity would impose delays as the intensity will not change immediately after a spike event. In the other direction, high frequency content of the firing intensity could make it impossible to translate the intensity back to spike trains. The performance disadvantage of using spikes to transmit information lie in the synapses, which need to translate the spikes into membrane currents. Before the reduction to rate-based models can be carried out, the behaviour of spiking models should be investigated in order to validate if the reduction is not degrading the accuracy of the models.

Choosing an appropriate model need to balance the gains and cost of the following three points

- The model should be sufficiently advanced to capture or investigate all the interesting aspects of the neuron from the perspective of the simulation that is carried out.

- The resources available from of the underlying hardware.

- There has to be enough experimental data to fit the model parameters.

The first point is self-evident, if the chosen model does not capture any of the interesting or sought-after characteristics of the system, the simulation has no purpose. It is a important point nonetheless, and it needs to be addressed when the model is created.

The resource demand of a model should also be considered, even though it is often hard to evaluate the strain on a large complex model merely by analysing the complexity of a single component. Looking at the Hodgkin-Huxley model and the four differential equations in Eq. (2.1), it could be argued that the model is too complex to be simulated efficiently. In the real case however, some neurons will receive synaptic input from more than a thousand axons. Each of theses synapses will be modeled by one differential equation, making the four differential equations in the Hodgkin-Huxley model seem rather bleak in comparison.

Still the bio-physical nature of the Hodgkin-Huxley model requires that many of the parameters and functions of the model have to be fitted through implicit methods, since the internal states, $m$, $n$ and $h$ can not be explicitly seen in ordinary experimental data. Instead of trying to describe the behaviour of a neuron as bio-physically accurate as possible, the phenomenological models that are described in the following sections, and used in this thesis, are constructed to emulate the behaviour of the neuron. Such an approach makes it more straightforward to fit the parameters of the models to the data. It also allows for expansions to handle complex neuron behaviour such as spike bursts, post-spike refractory periods and calculating membrane potential equilibriums.

## 2.1 Synaptic transmissions

As all neuron models used in this thesis transmit information through their generated spike trains, the behaviour of the synapse receiving a spike needs to be modeled. When a spike reaches the synapse from a another neurons axon, it triggers the release of chemicals called neurotransmitters. The neurotransmitters do in turn trigger the opening of ion channels through the targeted neurons cell membrane. Introducing the

state $r$ as the ratio between the number of open and closed channels, the conductance through the membrane due to the open channels can be described by Eq. (2.2).

$$g_i^{syn}(t) = \bar{g}_i r(t) \tag{2.2}$$

where $\bar{g}_i$ is the maximum possible conductance induced by the synapse. The behaviour of the state $r$ can be modelled by describing the transitions between the open and closed states of the individual ion channels. Introducing $\alpha$ and $\beta$ as the transition rates between the two states and $[T]$ as the concentration of neurotransmitters, the ratio $r$ can be defined as in Eq. (2.3).

$$\frac{dr}{dt} = \alpha[T](1-r) - \beta r \tag{2.3}$$

By approximating the release of neurotransmitters by pulses of size $T_{max}$ and duration $t_d$ at $t_0$, the following analytical solution to Eq. (2.3) can be found

$$r(t) = \begin{cases} r_\infty + (r(t_0) - r_\infty)\exp\left(-(t-t_0)/\tau_r\right) & t \in [t_0, t_0 + t_d] \\ r(t_0 + t_d)\exp\left(-\beta(t-t_0-t_d)\right) & t > t_0 + t_d \end{cases} \tag{2.4}$$

where

$$r_\infty = \frac{\alpha T_{max}}{\alpha T + \beta} \quad \text{and} \quad \tau_r = \frac{1}{\alpha T_{max} + \beta}$$

The outlined approach, described in detail in [Koch and Segev, 1998], has the advantage that it is simple, yet it is well behaved even during high synaptic activity. As some of the constructed networks have more than 10 times as many synapses than neurons, an efficient and simple model like this is required.

It should be noted than real synaptic activity is highly stochastic. The pulses of neurotransmitters will not be of the same size and there is no guarantee that the presence of neurotransmitter in the synaptic cleft will stimulate individual ion channels to transition between being closed to open [Hille, 2001]. Simulation of individual ion-channels are completely unrealistic and the stochastic nature of the channels can to some degree be compensated by other stochastic components of the network.

## 2.2 Fixed threshold models

All the models described in the following section are based upon the membrane potential as the fundamental state, just as the Hodgkin-Huxley model. The used approximations will however remove the implicit behaviour of generating action potentials. Instead, explicit methods for spike generation, involving fixed thresholds are introduced in all the models. The thresholds are chosen to emulate the behaviour of registered neurons, but having the thresholds fixed introduces problems when the input to the models forces the membrane potential to stay above a threshold for a long period of time. This limits the region where the model results stay valid, but is somewhat remedied by the soft thresholds introduced with the exponential integrate and fire model.

Furthermore, most neurons have a maximum fire rate caused by a refractory period after each spike during which no spikes are generated. In the escape rate models presented later on, the refractory period is implicitly built into the model, but the fixed threshold models need to keep track of the refractory period explicitly. This is

done by completely disregarding the spike generation thresholds during the refractory period.

**Integrate and fire**

Integrate and fire (IF) is one of the earliest and the most primitive models used to simulate spike generation within neurons [Abbott, 1999]. Even though it lacks many of the detailed characteristics describing a generic neuron, it still illustrates the conceptual behaviour of all neurons. It can also be seen as the first step towards more advanced phenomenological models. The membrane potential of the model is calculated by integrating the synaptic input, and as the potential reaches a fixed threshold, a spike is generated and the membrane potential is reset to the neuronŠs resting potential. The membrane potential of the IF model is described by

$$C_m \frac{dV_m}{dt} = I(t, V_m) \tag{2.5}$$

where $V_m$ is the membrane potential, $C_m$ the capacitance over the membrane and $I$ the current over the membrane. The current can either be a time-dependent bias or caused by open synaptic ion-channels that depend on the membrane potential. The total external current can thus be calculated by

$$I(t, V_m) = I_{bias}(t) + \sum_i g_i^{syn}(t) \left( V_m - E_i^{syn} \right) \tag{2.6}$$

where $E_i$ is the equilibrium potential for the ion-channel and $g_i$ the time-dependent conductance described in Eq. (2.2). Depending on the sign of the conductance, the synapse will either inhibit the target neuron by hyperpolarizing its membrane potential or excitate it by depolarizing the membrane. The resulting shape of the membrane potential shape is called an Excitatory Post Synaptic Potential (EPSP) or an Inhibitory Post Synaptic Potential (IPSP).

If addition to Eq. (2.5), the IF model also needs both a threshold, which determines whether or not a spike has been fired, and a reset potential, to which the membrane is reset after the spike has been fired.

**Leaky integrate and fire**

Even though simulating the ion channels through the cell membrane in detail might be going too far towards simulating the underlying biological system, the IF model lacks one basic aspect of the electrodynamic features describing the cell membrane. Since there is a conductance through the membrane, there will always be a leak current, pushing the membrane potential back to its equilibrium. Extending the IF model with a leak term leads to

$$C_m \frac{dV_m}{dt} = -g_L (V_m - E_L) + I(t, V_m) \tag{2.7}$$

where $g_L$ is the leak conductance over the membrane and $E_L$ the membranes resting potential or equilibrium where $I(t, V_m) = 0$. Due to the addition of a leak term this model is called Leaky Integrate and Fire (LIF). The leak term also ensures that Eq. (2.7) has a steady state solution, which can be seen as the membrane potential equilibrium. As it makes sense to reset the membrane potential to such an equilibrium after a spike has been generated, it is used instead of the explicit reset potential from the IF model. Using Eq. (2.6), the equilibrium of Eq. (2.7) becomes

$$V_{eq} = \frac{1}{g_L - \sum g_i^{syn}} \left( I_{bias} + g_L E_L - \sum g_i^{syn} E_i^{syn} \right) \tag{2.8}$$

**Exponential integrate and fire**

Both of the previous models are based on the assumption of a static capacitance and conductance of the cell membrane of the neurons. As the conductance of the different ion channels of the membrane is not static, but varies with several different enviromental factors, some of the behaviour of the neurons is not captured using the models above. The most obvious such behaviour is the generation of spikes, which is triggered by depolarization, leading to a cascade of sodium channels opening and generating a spike trough the resulting rapid depolarization.

The Exponential Integrate and Fire model (EIF) [Fourcaud-Trocme *et al.*, 2003] shown in in Eq. (2.9), mimics this behaviour by introducing another term into Eq. (2.7), imitating the current caused by the cascade of opening channels. The simulated depolarizing cascade is initiated when the membrane potential, $V_m$ grows larger than the threshold $V_t$ and the speed of the cascade can be modified by $\Delta_T$.

$$C_m \frac{dV_m}{dt} = -g_L (V_m - E_L) + g_L \Delta_T \exp \left( \frac{V_m - V_t}{\Delta_T} \right) + I(t, V_m) \tag{2.9}$$

As the growth introduced by the additional term is large enough to reach astronomical values within a time-step of simulation, no explicit firing threshold is needed. Instead, a spike is considered to be generated whenever the membrane potential reaches out of bounds. In order to comply with the refractory period from the modeled neuron, the exponential term cannot be used during the refractory period following a generated spike. The resulting model exhibits close to identical timing of generated spike compared with the Hodgin-Huxley model [Fourcaud-Trocme *et al.*, 2003], which makes it a suitable phenomenological model to use.

Using the membrane potential within the exponent of added term, leads to the implicit formula for $V_{eq}$ in Eq. (2.10). The equation can be solved for $V_{eq}$ numerically, using the Newton-Raphson method with the equilibrium from the LIF model as an initial predictor value. Because of convergence issues, a diverging result is discarded and replaced with the equilibrium of the LIF. This approach has yielded good enough results, but a algorithm which always converges would of course improve the behaviour of the model in the few cases where the iterations diverges.

$$V_{eq} = \frac{1}{g_L - \sum g_i^{syn}} \left( I_{bias} + g_L E_L + g_L \Delta_T \exp \left( \frac{V_{eq} - V_t}{\Delta_T} \right) - \sum g_i^{syn} E_i^{syn} \right) \tag{2.10}$$

**Integrate and fire or burst**

Some neurons exhibit more elaborate spike patterns than those generated by the previously described models. Bursting neurons fire bursts or clusters of spikes with short Inter Spike Intervals (ISI), while the ISIs between the bursts can be several times longer. The biophysical cause of this behaviour is most likely calcium ($Ca^{2+}$) channels that open during bursts leading to depolarization, forcing additional spikes to be generated with short ISIs until the calcium channels are depleted and the burst stops.

The Integrate and Fire or Burst (IFB) model from [Smith *et al.*, 2000], models this with calcium channels, whose membrane current contribution is described by Eq. (2.11). The activity of the channel is governed by the state $r_{Ca}$ in Eq. (2.12).
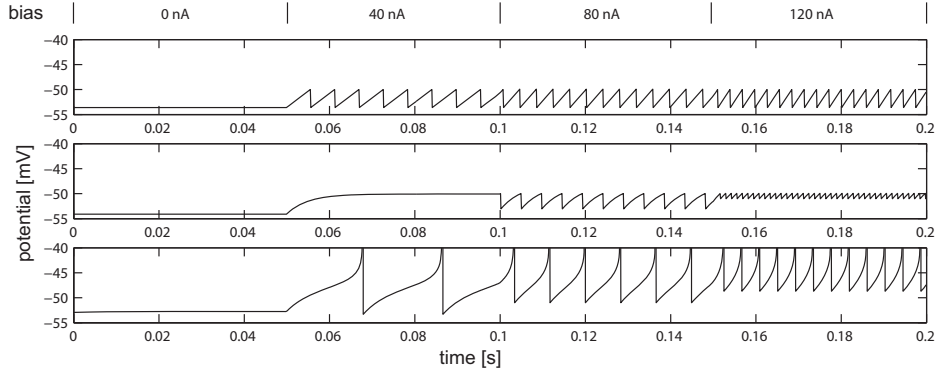
**Figure 2.1** Simulation of a IF, LIF and EIF model.

When the membrane potential reaches above $V_{Ca}$ the ion channels open, causing extra depolarization, and at the same time $r_{Ca}$ starts to deplete. In order for $r_{Ca}$ to be replenished, the membrane potential has to fall below $V_{Ca}$ again.

$$I_{Ca}(t, V_m) = \bar{g}_{Ca} r_{Ca}(t) H(V_m - V_{Ca})(V_m - E_{Ca}) \qquad (2.11)$$

$$\frac{dr_{Ca}}{dt} = \begin{cases} -r_{Ca}/\tau_{Ca}^- & V_m > V_{Ca} \\ (1 - r_{Ca})/\tau_{Ca}^+ & V_m < V_{Ca} \end{cases} \qquad (2.12)$$

where $H$ denotes the Heaviside function.

The IFB model can be extended with the exponential part of the EIF model, creating an Exponential Integrate and Fire or Burst (EIFB) model instead. Using the basic EIFB setup, the external input to the neuron has to allow the membrane potential to fall below $V_{Ca}$, or no new bursts will be generated. In the EIFB simulation shown in Fig. 2.2, the bias current applied to the model does not allow the membrane potential to fall back below $V_{Ca}$, leading to just a single burst just after the bias current is first introduced. To manage this, some neurons will actively hyperpolarize their membrane potential after a burst, by activating strong hyperpolarizing potassium ($K^+$) channels. The potassium channels can be modeled as synaptic ion-channels described in Eq. (2.6), but instead of reacting to incoming spikes it releases its neurotransmitters whenever $r_{Ca}$ is below the threshold $\varepsilon_{Ca}$ at the same time as a action potential is generated by the neuron. Simulation results where the potassium channels are incorporated into the EIFB model can be seen in Fig. 2.2.
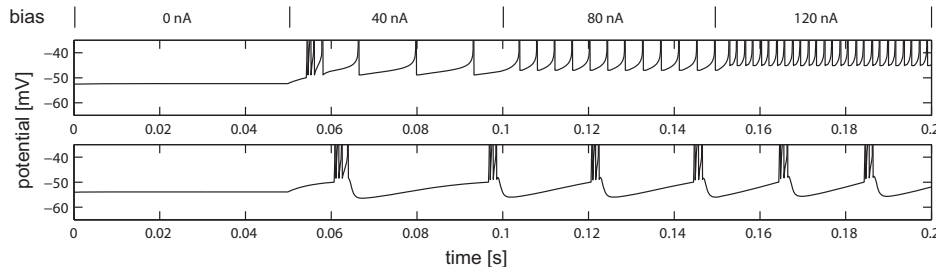


**Figure 2.2** Simulation of an EIFB, with (below) and without (above) the simulated potassium channels. Notice how the model only bursts once during the simulation when the potassium channels are not used.

11

## 2.3  Escape rate models

The models that have been described so far, where the action potentials of a neuron is generated by explicit thresholds or equations describing the membrane potential during the generation of a spike, are the most frequently and successfully used to model real neurons. In order to mimic the random behaviour of the modeled neurons, they can be further extended with stochastic terms in the various equations, creating stochastic differential equations [Saarinen *et al.*, 2008].

As the purpose of the models used in this thesis is to construct networks of neurons, and not to study the individual neuron in great detail, information about the actual behaviour of a neuron during a spike is not needed. Assuming that neurons only communicate by discrete spikes with no inherent information but the time they were generated, the actual information needed from a single neuron model to describe the behaviour of the entire network can be drastically reduced. Instead of simulating the actual behaviour of the membrane potential, some basic relationship between input spike patterns and output spike patterns could be used to construct even simpler models.

When the spike patterns of some types of regular neurons are examined, they exhibit a high amount of spikes even during rest, when they receive no synaptic input. This can be modeled using stochastic differential equations, but a more straightforward approach would be to describe the spiketrains using statistical methods. This has been thoroughly covered using point process or Escape Rate (ER) models in [Dürango, 2010], and the results from that work is used to motivate the models chosen for some of the neurons. The remaining part of this chapter will describe how such ER models can be used to describe the generated spike pattern in relation to synaptic input, establishing a simple input output relationship of the modeled neuron.

**Renewal processes**

If the ISI following a spike can be determined without any knowledge of prior spike times, the spike train can be described by a renewal point process. The activity of such a neuron at rest is fully described by its ISI Probability Density Function (PDF). By choosing a skewed distribution, such as the gamma or log-normal distribution, the PDF will implicitly handle the refractory period following a generated spike as almost no extremely short ISIs will be generated. The skewed shape of the log-normal distribution can be seen in Fig. 2.3.

Since the log-normal distribution described in Eq. (2.13) is shown to fit measured ISI distributions sufficiently well in [Dürango, 2010], no other distributions are used during the this thesis. The assumption that the ISIs can be modelled as renewal processes are both validated and invalidated for different neurons of the same type in [Dürango, 2010]. This should be noted and is worth investigating, but is not researched any further other than for neurons which exhibit bursting behaviour.

$$f(x|\mu,\sigma) = \frac{1}{x\sigma\sqrt{2\pi}} \exp\left(\frac{-(\ln x - \mu)^2}{2\sigma^2}\right) \qquad (2.13)$$

**Non stationary processes**

Using the previously outlined methods, a neuron at rest or with a static bias can be simulated using a single distribution describing its ISIs. As all real neurons work under non-stationary conditions, the shape of the distribution has to be related to the synaptic input of the neuron. The log-normal distribution is fully described by the underlying normal distributionŠs mean $\mu$ and standard deviation $\sigma$, which calls for
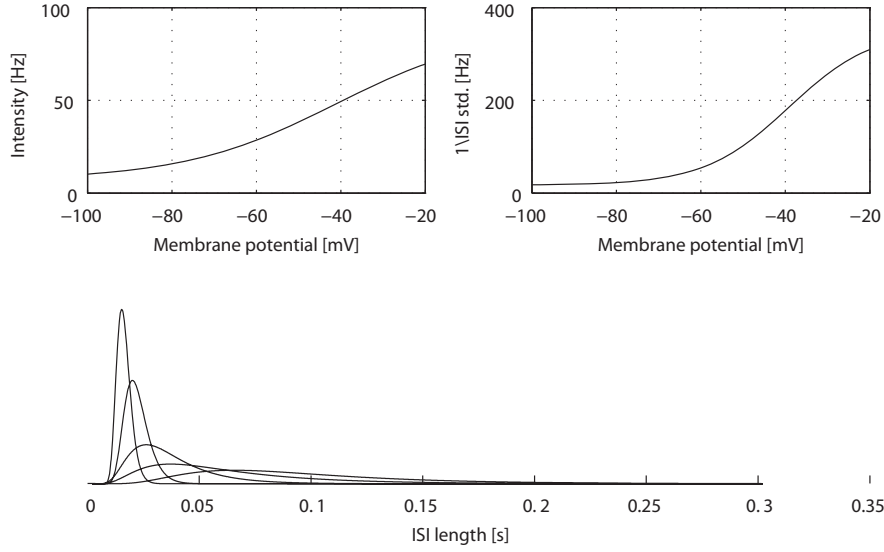
**Figure 2.3** Example distributions and sigmoid curves. The PDFs are constructed using mean and standard deviation values from the two curves at -60, -54, -52, -50 and -45 mV.

relations between those variables and the membrane potential of the neuron. As $\mu$ and $\sigma$ are variables of the underlying normal distribution, it is more straight forward to relate the mean and standard deviation of the actual log-normal distribution to the membrane potential. The pairs can be transformed between each other with the help of Eq. (2.14).

$$
\begin{aligned}
\mathrm{E}\left[X\right] &= \exp\left(\mu + \frac{1}{2}\sigma^2\right) \\
\mathrm{Var}\left[X\right] &= \left(\exp\sigma^2 - 1\right)\exp\left(2\mu + \sigma^2\right)
\end{aligned}
\tag{2.14}
$$

where X is a stochastic variable from the log-normal distribution.

A common way to relate the activity of a neuron to its input is to use its spike rate, which equals the inverse of the ISI mean. In the operative range of the neuron, the relationship between a current bias and the intensity can be approximated as linear. However, when the input reaches outside of the operative range, the intensity saturates and reaches a maximum firing frequency diverging from the linear approximation. Similarly the intensity reaches a minimum firing frequency or zero when the input bias falls below the operative range.

In order to model the behaviour when the intensity saturates, the linear approximation can be exchanged against a sigmoid shaped curve. The curve generated by Eq. (2.15) has the advantage that the parameters, $p_1$ to $p_4$, explicitly give some features of the curve. Here, $p_1$ equals the minimum intensity asymptote and $p_1 + p_2$ equals the maximum intensity asymptote, while $p_3$ and $p_4$ determine the shape and slope of the linear region.

$$
I\left(V_m\right) = p_1 + \frac{p_2}{1 + \exp\left(p_3 - V_m\right)/p_4}
\tag{2.15}
$$

The complete neuron model is given by two sigmoid curves as the one above. One which gives the intensity and thereby the ISI mean and one which gives the inverse of

the ISI standard deviation. Using them, a distribution describing the firing behaviour of the neuron can be constructed at any synaptic or bias input. In Fig. 2.3, such a model has been fitted to real neuron data.
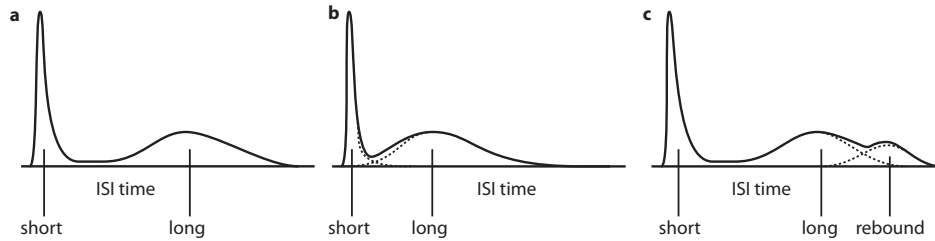
**Bursting neurons**



**Figure 2.4**    Three example multimodal PDFs from spiketrains containing bursts. **a)** Bimodal PDF where the two underlying distributions (short and long) are well separated and can be separated by a simple threshold. **b)** The two underlying distributions partly overlap making it harder to separate them. **c)** Contains a third distribution (rebound) e.g. caused by the high hyperpolarizing rebound following a burst.

Since bursting neurons also exhibit spontaneous and stochastic activity, there is reason to extend the basic ER model to enable it to emulate bursting neurons as well. Fig. 2.4 illustrates some different distributions of ISIs that bursting neurons can exhibit. The distributions show at least two peaks, one from the short ISIs during bursts and one for the long ISIs between bursts. If such a histogram can be constructed from measurements of the neuron, the shape of the histogram could be described by one unimodal distribution for each peak.

If the process is strictly renewal, the model could be constructed by superimposing several distributions on top of each other, constructing a multi-modal PDF that can be used in an ordinary ER model. If the process is not a renewal process, as most of the investigated bursting neurons will be shown to not to be, the model has to be extended.

This can be done by using a Hidden Markov Model (HMM) with at least two states, one for regular firing, and one for bursts. Different burst lengths can then be modeled by introducing more states, modeling the probability of different burst lengths through the state transition probabilities as in Figs.2.4 **a-b**. Some bursting neurons with an extra strong hyperpolarizing rebound do show a third peak in their ISI histograms as in Fig. 2.4 **c**. This behaviour can be included to the model with another state, where the ISI is picked from the third distribution. This could of course be used for all peaks, as long as the transition probabilities can be determined.

To simplify the visualization of the models, discrete distributions determining the length of bursts or periods without bursts can be constructed, reducing the amount of states to one for each peak in the original PDF. Whenever such a state is reached, the amount of successive ISI from that states PDF is picked from its discrete distribution. Figs. 2.5 **a-b** show two different HMMs and their corresponding burst length distribution. This method has been successfully employed in [Ekholm and Hyvärinen, 1970], where methods to separate overlapping peaks as those in Fig. 2.4 **b** are also discussed.

The advantage of using an ER model to model bursting neurons is the models ability to explain spontaneous activity, and that it does not depend on any artificial fixed thresholds. The main problem with them is to fit them to non-stationary processes, as much more data is needed in order to find the different PDFs and how they

in turn depend on the current membrane potential of the neuron. The experimental data, measured at different induced membrane potentials, do also have to be collected during stationary conditions. This might lead to a loss of important dynamics if it is not done carefully.
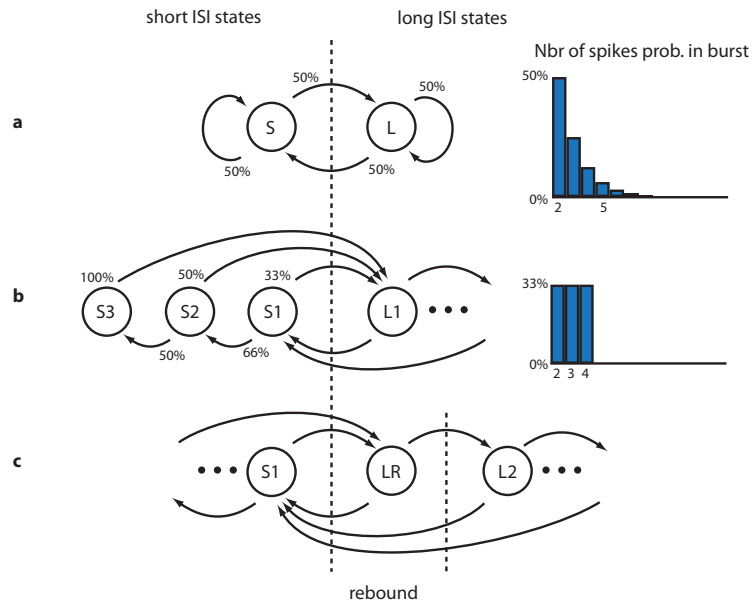


**Figure 2.5**   Different configurations of the Markov models. **a)** The model has two states, S picks short ISIs and L picks long ISIs. Note the exponential decay of the nbr. of spike probability. **b)** Additional short states, S1 - S3, are introduced to create a equal probability for bursts containing 2, 3 and 4 spikes. **c)** A rebound state LR is introduced which picks ISIs from the rebound distribution (see Fig. 2.4 **c)**
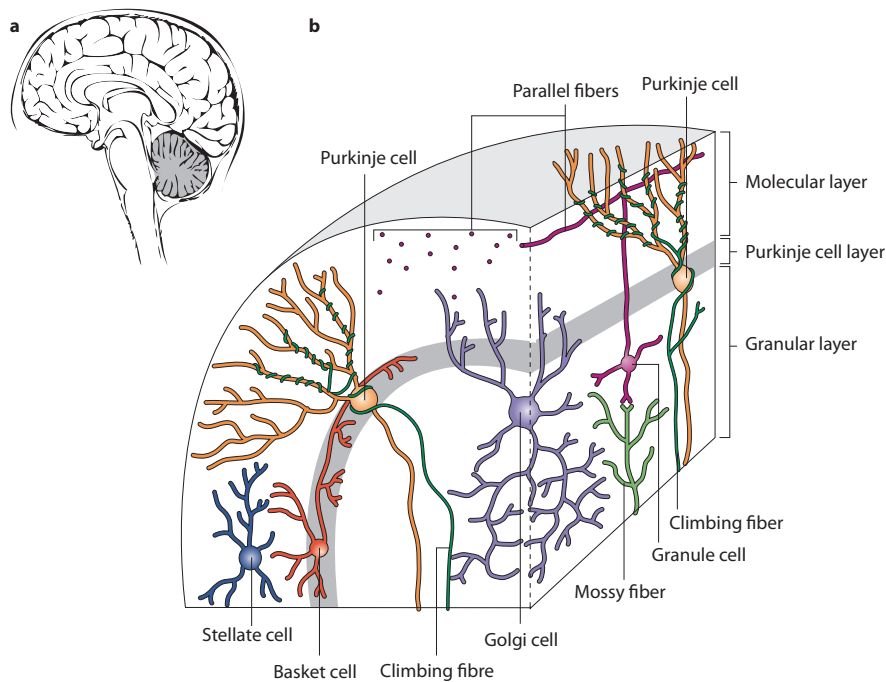
# 3. The cerebellar topology



**Figure 3.1** **a)** The gray area is where the cerebellar cortex is located within the human brain. **b)** The overall structure and different types of neurons within the cerebellum. [Purves *et al.*, 2004]

While the cerebellum contains billions of neurons, its neural circuitry demonstrates a surprisingly simple structure. Its general structure has lead to the belief that it should be possible to characterize the exact function of the cerebellum as it seems to be involved in a wide range of task within the brain, from motion control to internal models explaining intuition and implicit thought [Ito, 2008]. All the different neurons types and their position within the layers of the cerebellum can be seen in Fig. 3.1 **b**.

The cerebellum receives input through two different neural pathways. The first carry afferent sensory information and efferent motor commands through several million mossy fibers, reaching the granule cells within the granular layer [Ito, 1984]. The second source is through Climbing Fibers (CF) that originate from the Inferior Olive (IO), and terminate in the molecular layer, where they innervate Purkinje cells with multiple synapses climbing through the dendritic tree of the Purkinje cells. The Purkinje cells do finally send axons to the Deep Cerebellar Nuclei (DCN), constituting the only output from the cerebellum [Ito, 1984].

## 3.1 Mossy fibers

The Mossy Fibers (MF) originate from the pontine nucleus, the spinal cord and the vestibular system. The signals from the vestibular system are involved in the vestibu-ocular reflex, which is a thoroughly studied control loop where the cerebellum is the main controller, regulating the eye position in order to obtain stable vision [Ito,

1984; Kawato and Gomi, 1992; Schweighofer *et al.*, 1996]. The signals from the pontine nucleus carry efferent motor commands from the motor cortex, while all afferent proprioceptive and tactile sensory information is carried through the spinal cord and cuneate nucleus. Some of the mossy fibers also form collaterals directly to the DCN, but that is beyond this thesis.

**The cuneate nucleus**

Even though no afferent sensory information is used in the complete simulated network, the individual neuron models are validated against data derived through *in vivo* measurements of the different neurons during tactile stimulation. In order to capture that behaviour and also investigate the information processing capabilities of the cuneate nucleus, the cuneate neurons and their behaviour is also investigated and modeled.

The cuneate nucleus receive afferent tactile information through primary afferents, which innervate cuneate neurons. The cunate neurons do in turn send axons becoming mossy fibers that reach the cerebellar granular layer. Other than the synaptic connections between primary afferents and cunate neurons, the cuneate nucleus also contains inhibitory interneurons which are also innervated by the primary afferents. They do in turn form inhibitory synapses against the cuneate neurons [Bengtsson *et al.*, 2011].

In this thesis, the cuneate neurons make up the periphery of the simulated network. Even though the interactions between interneurons and primary afferents are interesting from a feature extraction standpoint, it is not investigated further. Instead, recorded spiketrains from both interneurons and primary afferents are fed to the network making it superfluous to investigate their behaviour or model them.

The cuneate neurons do on the other hand show interesting behaviour that is further investigated. The spike trains they generate during tactile stimulation of their receptive fields do often, but not always, contain bursts [Sánchez *et al.*, 2006]. Their resting potential does also lie very close to their firing region, with a fair amount of spontaneous activity as a result. The combination of these two features mean that they react with a substantial activity even with small primary afferent input. This makes them ideal for reacting to small sensory changes [Bengtsson *et al.*, 2011].

**Efferent trajectory references**

There is evidence that the desired trajectory of planned movements is generated within the central nervous system and reaches the cerebellum through mossy fibers. The signal shows little correlation with load disturbances applied to the limbs involved in the motion, which suggests they encode the desired trajectory and not actual motor commands, which must include the disturbances in order to be able to compensate for them [Schweighofer *et al.*, 1998, II].

The signals have been shown to correlate with both the desired position and velocity and the activity of some cells appears to be related to acceleration. As the desired position, velocity and acceleration are all needed by an inverse model, this corroborates the view where the cerebellum is seen as a feed forward controller that compensate for both poor original control and disturbances from external factors.

## 3.2   Granular layer

All of the MFs that reach the cerebellum terminate in the granular layer in glomeruli, where they innervate both granule cells and Golgi cells. A simplified illustration of
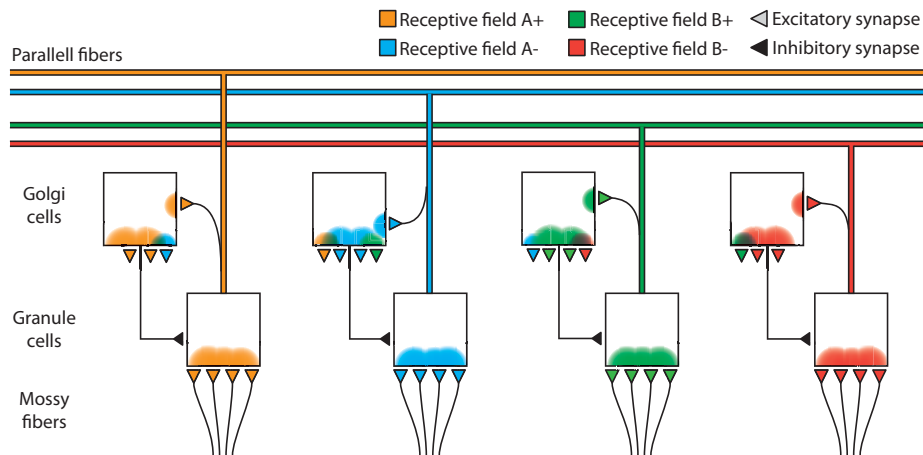
**Figure 3.2**   Simplified structure of the granular layer

the connection pattern can be seen in Fig. 3.2, where emphasis was put to the receptive fields of the different granule cells and their neighbouring Golgi cells.

In the somatosensory system, a receptive field can be a certain skin area or a region of an internal organ. The four different receptive fields in the figure, denoted $A+$, $A-$, $B+$ and $B-$, are thought to receive their input from tactile sensors on skin areas close to two different joints $A$ and $B$. The two receptive fields of each joint is located opposite each other, thus having opposite reactions to changes in joint angles. When the $+$-area is stretched, the $-$-area will contract. This feature leads to important evidence of the cerebellar function later on in this chapter.

As mossy fibers carrying signals from the same receptive field or modality reach the cerebellum together, they innervate the same granule cells and they will in turn carry information from those receptive fields through their axons up to the molecular layer [Bengtsson and Jörntell, 2009]. In the molecular layer, the granule cell axons turn into parallel fibers (PF).

**Granule cells**

The cerebellar granule cells are among the smallest neurons in the brain and also the most numerous. A human brain contains around 10 to 100 billion granule cells and occupy roughly one third of the cerebellar mass. The great number of granule cells compared to the number of incoming MFs leads to each MF innervating around 2000 granule cells, while each granule cell only receives input from 4-5 different mossy fibers [Ito, 1984].

The large amount of granule cells carrying the same information as the much less numerous incoming MFs, does also point towards some kind of signal transformation capabilities within the glomeruli. This is one of the corner stones of the adaptive filter interpretation discussed later on in this chapter.

As opposed to the cuneate neurons that fire at the slightest depolarization, the granule cells have resting potentials that lie much lower than the region where they start to form action potentials. In order for them to reach that region they require that at least two of the MFs that innervate them fire simultaneously. This feature could be used to filter out spontaneous MF activity [Dean *et al.*, 2010] or as a method to extract features from the MF signals. There are also evidence of other feature extracting capabilities within the glomeruli, including high-pass and low-pass filtering [Mapelli *et al.*, 2010].

**Golgi cells**

Golgi cells are located together with the granule cells in the granular layer. They have an inhibitory effect on the granule cells and receive excitatory synapses from MFs and also back from the granule cells, both in the granular layer and from parallel fibers in the molecular layer. The Golgi cells achieve the inhibitory effect by forming synapses onto the mossy fiber granule cell excitatory synapse, modulating the strength of the synapse. The strongest input synapses are made by mossy fibers, of which the majority arrive from the same receptive field [Palay and Shan-Palay, 1974; D'Angelo, 2008; Jörntell and Ekerot, 2006].

The inhibitory effect upon the granule cell activity permits the Golgi cell to regulate the intensity of the granule cells it innervates, keeping them from being completely quiet or saturated due to low or high input from the surrounding mossy fiber and granule cell activity [Dean *et al.*, 2010]. This allows the granule cells to stay within their preferred region of activity.

Moreover, the strength of the inhibitory effect varies with the distance between the inhibited granule cell and the Golgi cell, which is called the center-surround effect [D'Angelo, 2008]. This will keep the activation threshold of all granule cells in the vicinity to a Golgi cell varied, something that could be of use to extract features from the mossy fiber signals.
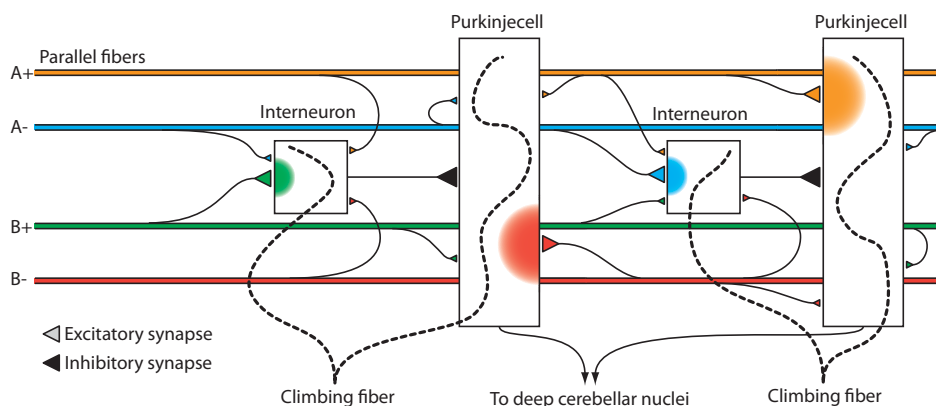
## 3.3  Molecular & Purkinje cell layer



**Figure 3.3**   Microcircuitry within the molecular and Purkinje cell layer

**Basket & stellate cells**

Other than the parallel fibers and dendritic trees of the Purkinje cells, the molecular layer also contains interneurons that form inhibitory synapses upon the Purkinje cells and also to some extent each other. They are usually divided into basket cells and stellate cells due to their location and the appearance of their dendritic trees and axons, illustrated in Fig. 3.1 on page 16 [Palay and Shan-Palay, 1974].

Their difference in appearance has given rise to some proposed differences of their function within the cerebellar microcircuitry. The widespread dendrites of the basket cells along the Purkinje cell layer are proposed to collect information from a larger receptive field than that of the Purkinje cells, enabling different types of feature extraction [Schweighofer *et al.*, 1998; Kitazawa *et al.*, 1998]. The interneuron

cell bodies are spread across the molecular layer, but can be labeled as (*1*) deep (*2*) middle and (*3*) superficial , to describe their depth within the layer and space they occupy with their dendritic arbors [Ito, 1984].

Recent studies have shown that the stellate and basket cells share the same receptive field. They have also been found to share the same basic properties, both regarding their membrane parameters and the parallel fiber input synapse characteristics [Jörntell *et al.*, 2010]. This leaves different connectivity patterns to be explored. The activity from a superficial stellate cell recorded during *in vivo* experiments shown in Fig. 3.4 exhibit some interesting behaviour that must be due to the incoming inhibitory synapses from other interneurons. A short time after the tactile stimulation the interneuron becomes quiet, seemingly inhibited by another interneuron.

There are no detailed investigations into which connection patterns that do exist within the molecular and Purkinje cell layer. The basket and stellate cells do at least innervate the Purkinje cells with inhibitory synapses [Schweighofer *et al.*, 1998, II], but the data in Fig. 3.4 indicate that there are also inhibitory connections between the interneurons. This is corroborated by dyed basket cells which show axons reaching into the molecular layer [Palay and Shan-Palay, 1974]. The most efficient way for the basket cells to innervate the Purkinje cells would be within the Purkinje cell layer, indicating that the basket cells reach for stellate cells within the molecular layer and not the dendritic trees of the Purkinje cells.

Innervating superficial stellate cells with basket cells is most likely not enough the explain the data in Fig. 3.4. The innervating basket cell do in some sense also need to be slower than the stellate cell to delay the main inhibitory effect until around 100 ms after the stimulation onset, which is when the superficial interneuron in the figure goes quiet.
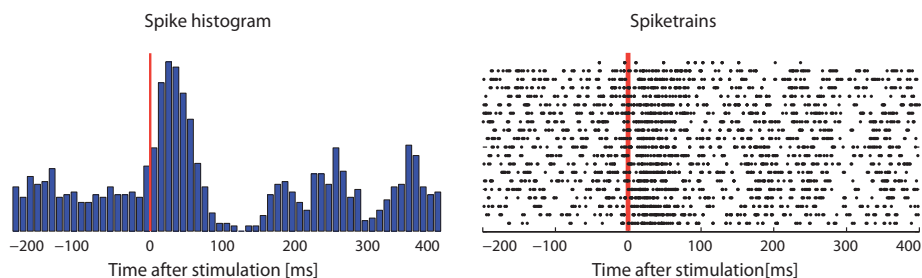


**Figure 3.4**   Spiketrains registered from a stellate interneuron during tactile stimulation and a histogram combining them.

**Purkinje cells**

Purkinje Cells (PC) are one of the largest neurons within the human brain. They are innervated by up to 200,000 parallel fibers that pass through their dendritic trees in the molecular layer. Furthermore, both basket cell and stellate cell interneurons provide inhibitory input. In addition to the input originating from the mossy fibers, climbing fibers from the inferior olive innervate 1 to 10 different Purkinje cells forming several excitatory synapses onto each of their synaptic trees. The Purkinje cells are however only innervated by a single climbing fiber each [Ito, 1984].

During periods without climbing fiber activity, Purkinje cells generate action potentials at rates between 17-150 Hz, with a non-negligible spontaneous activity at 40 Hz on average [Dean *et al.*, 2010]. The simple spikes are interrupted whenever the climbing fiber is activated. Instead, due to the CFs many synapses and strong excita-

tory effect, the Purkinje cell fires a complex pattern of spikes, followed by a period of suppressed spontaneous activity.

Climbing fiber activity has also been shown to modify the synaptic strengths of parallel fiber synapses innervating the Purkinje cells, but also nearby interneurons that are innervated by climbing fiber collaterals [Jörntell and Ekerot, 2003].

The actual distribution of those weights, measured during *in vivo* experiments and illustrated in Fig. 3.3, show patterns that corroborate the adaptive filter hypothesis. Many of the synapses are silent with negligible strength, but more importantly, if the PF carrying signal from a receptive field have strong PC synapses ($A+$ and $B-$), the PFs with the opposite receptive fields ($A-$ and $B+$) will have strong synapses against the interneurons innervating the PC [Jörntell and Ekerot, 2002]. Such a configuration is what would be expected from an adaptive filter with positive weights and explicit sign changers.

## 3.4 Cerebellar microzones

The connection pattern of both the climbing fibers, the parallel fiber receptive fields and the projection of the Purkinje cells upon the DCN allows for the partition of the cerebellar cortex into microzones [Dean *et al.*, 2010]. Fig. 3.5 shows where such a microzone could be located within a unfolded part of the cerebellar cortex. Note how the Purkinje cell dendritic tree spreads perpendicularly to the parallel fiber direction.
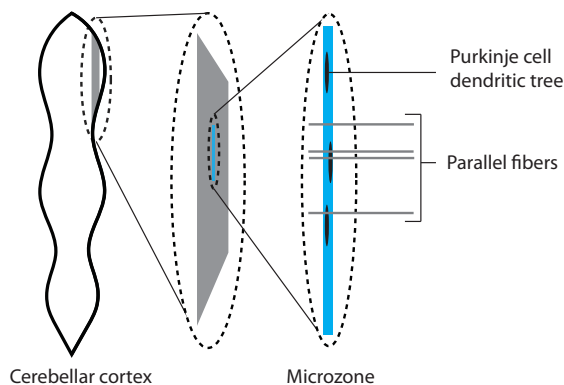


**Figure 3.5** The organization of cerebellar microzones within the cerebellar cortex

Each microzone contains a couple of hundred Purkinje cells. They are located in strips that lie perpendicular to the direction of the parallel fibers. Each parallel fiber will thus reach through several microzones. Due to the placement and size of the microzones and the incoming MFs, the microzones mostly receive input from the same receptive field [Jörntell and Ekerot, 2006].

What defines the microzone is its incoming climbing fibers. As each climbing fiber does contact 10 different Purkinje cells, each microzone receives several climbing fibers. They all originate from the same area in the inferior olive, where the inferior olive neurons terminating in the same microzone are coupled by electrical gap junctions, synchronizing their spiking behaviour [Dean *et al.*, 2010; Schweighofer *et al.*, 2004]. Finally the axons from Purkinje cells within the same microzone terminate at the same location within the DCN, which implies that their output is somehow converging there and is used to control the same system outside of the cerebellum [Dean *et al.*, 2010].

## 3.5 Plasticity of the parallel fiber synapses

The long term effect the climbing fiber activity has on the synaptic strength of the PF synapse, both against the Purkinje cells and interneurons, makes it important to investigate the information content sent though the climbing fibers.

The most striking feature of their activity is their unusually slow firing rate. Usually the IO neurons do not fire much more than one time each second. If the signal is only used to modify the synaptic strengths, the slow firing rate could be to avoid interfering with the actual motor control [Schweighofer *et al.*, 2004]. On the other hand, there is evidence the climbing fiber signal is used to initiate movements, sending a spike at the onset of the movement [Kitazawa *et al.*, 1998].

Since climbing fiber activity also leads to plasticity of the PF synapses, assuming the cerebellum is used to correct compound motions, the climbing fiber signal should code for the error during the movements. This will essentially decorrelate the Purkinje cell output with the motion error, improving the motor control the next time the motion is performed. The signal has been shown to contain both the target position at the onset of movement, and the error as the motion is completed, corroborating both the hypotheses [Kitazawa *et al.*, 1998]. The spike at onset of movements is explained as an acceleration error by [Schweighofer *et al.*, 1998, I], but this assumes the error calculation uses actual values with fairly large delays.

In [Kitazawa *et al.*, 1998], the initial signal is both correlated to the end position and shown not to be calculated through vision feedback by obscuring the movement from the subject of the experiments. The end position is however related to the initial acceleration, and assuming that proprioceptive and tactile feedback can be used to calculate the error, it could still be some kind of error signal. It should be noted that the two options are in no way mutually exclusive as there is no apparent reason the cerebellum could not be used for both tasks.

Since all signals through the nervous system suffer from substantial delays, excluding the even longer delays caused by the muscle system, an adaptive controller needs to account for those delays in order for the adaptation to be stable. The plasticity of the PF synapses shows some evidence of such a behaviour. The timing between PF activity and CF activity play a crucial role in determining the size of the synaptic update, where the order of activation also matters [Sarkisov and Wang, 2008]. In simulations, delays between 50ms [Schweighofer *et al.*, 1998, II] and 150 ms [Schweighofer *et al.*, 1996] have been used successfully to train networks.

The slow rate of spikes through the CFs does of course deteriorate the information content of the transmitted signal. In [Schweighofer *et al.*, 2004] small regions of the IO were simulated to investigate the characteristics of the CF signals. It was shown that chaotic elements generated by the electrical gap junctions between the IO neurons increased the information content of the signal during the simulation. No model of the IO is constructed during this thesis, but it would be a natural extension in order to investigate the behaviour of the CF signal.

## 3.6 Cerebellum as an adaptive filter

Both the anatomical structure of the cerebellum and the synaptic configurations of PF synapses from *in vivo* studies have lead to the idea that the cerebellum works as an adaptive filter [Dean *et al.*, 2010; Fujita, 1982; Ito, 1984]. Fig. 3.6 shows the how the basic structure of the cerebellum can be transformed into a basic adaptive filter, while the apparent receptive field specific weight distributions seen in Fig. 3.3 gives

evidence of actual training. As both LTD and LTP of PF synapses exist, both upon interneurons and Purkinje cells, most of the fundamental criteria required to build the adaptive filter structure in Fig. 3.6 are met [Dean *et al.*, 2010].
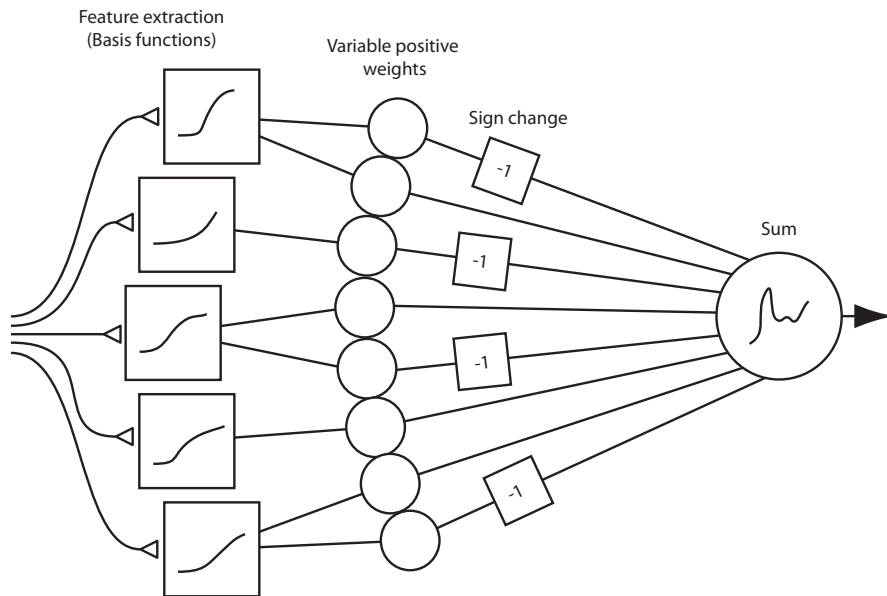


**Figure 3.6**   Adaptive filter interpretation of the cerebellar function

Since the synaptic weights are not allowed to change sign, they are either inhibitory or excitatory, the interneurons play a crucial role in allowing the signals carried by the PF to have an inhibitory effect upon the Purkinje cells. Furthermore, the plasticity of of the PF synapses upon the interneurons are reversed compared to those innervating the Purkinje cells [Jörntell *et al.*, 2010]. This gives further evidence of the adaptive filter hypothesis.

In order for the filter to create the inverse models necessary for motor control, it also has to be able to approximate non linear functions. This could be attributed to the granule cells if they can be shown to perform transformations from input spike rate to output spike rate, resembling some kind of basis functions. This would also explain the abundance of granule cells.

Depending on the input available, some derivative and integrating action might also be required. Some signs of such capabilities has been found in the cuneate nucleus [Forsberg, 2010], where derivative action was found by analysing histograms obtained from *in vivo* experiments. Derivative action has also been attributed to the interactions between mossy fibers and granule cells [Fujita, 1982]. It has also been shown that some granule cells receive functionally equivalent input from all four mossy fibers, indicating that they function as coincidence detectors, gating out noise from the mossy fibers [Bengtsson and Jörntell, 2009].

Because of the slow Golgi cell behaviour, they could be involved in integrating action [D'Angelo, 2008], and also in low pass filtering of the MF inputs [Fujita, 1982]. Their center-surround effect upon the strength of the synapses between MF and granule cells could also be used modulate the activity of the granule cells creating a large set of different basis functions that could be used by the Purkinje cells to approximate non-linear functions.

It is tempting to see the adaptive filter interpretation of the cerebellar function

as the final model of the cerebellar function. A generic adaptive filter is, just like the cerebellum, extremely versatile, and can be used to approximate a wide range of different functions and systems. It does however move much of the responsibility to the teaching signal, which in the cerebellum is attributed to the CF signals. The nature of that signal is still controversial, and while there is evidence of correlations with movement errors, much of the higher level abstract models assume the kind of teaching signals that corroborate their model. This includes the plasticity model from [Schweighofer *et al.*, 1998, II] which is used in this thesis in a slightly modified form.

The adaptive filter does also require a higher-level model to explain how motor control is possible, as one single inverse model cannot be used in all situations, counteracting different external force-fields or loads applied to the controlled limb. Yet the nervous system can manage instantaneous switches between different external force-fields without loss of control performance [Yamamoto *et al.*, 2007]. The model in [Kawato, 1999] tries to explain how this is accomplished. It uses several cascaded inverse and forward models to switch between different situations depending on special contextual signals.

Both the issue regarding the CF signal and possible higher-level abstractions are important research topics, whose answers will greatly improve the understanding of the cerebellar function. They are however beyond the scope of this thesis.

# 4. Simulation setup

The purpose of this thesis work is to develop the basis of a cerebellar simulation toolkit that can be used to investigate cerebellar behaviour involving up to thousands of neurons forming large networks. The path to reach such a goal can be divided into the following tasks, divided into two subsequent steps.

1. Model individual cerebellar neurons

   (a) Choose the basic model that should be used for each cerebellar neuron type based upon their known behaviours.

   (b) Fit the model parameters to experimental data.

   (c) Validate the simulation results against experimental data during standardized afferent input.

2. Use the neuron models to construct networks, investigating the behaviour of neurons in concert.

   - Investigate subsets of the cerebellar micro circuitry to examine different hypotheses of cerebellar function.

   - Construct a complete network and train it to perform a simple task, enabling analysis of neural pathways through the entire cerebellum.

Even though the first step deals with individual neurons and how to model them, small networks has to be created to be able to validate the models. This is mainly due to that the afferent input used for validation has to pass through all prior neurons before it reaches the neuron in question. In some cases though, the network structure can be seen as a part of the neuron model in order to fit the simulation results to the validation data.

During the second step a complete network is created, built upon the structure from [Schweighofer *et al.*, 1998, II], where the network is trained to mimic the inverse dynamics of a double joint arm. The overall network structure, the number of neurons and the number of synapses used in the network are similar to that used in the Schweighofer article, but the following main differences exist

- Spiking neuron models are used instead of rate-based models

- No muscle model is used.

- The generated trajectory is generated in joint space.

- No afferent input is used as it would contain the same information as the generated trajectory, but delayed.

- Other than the LTD of PF-PC synapses modelled in [Schweighofer *et al.*, 1996], LTP of PF-PC synapses and LTD/LTP of PF-interneuron synapses are added leading to another weight normalization rule.

- In [Schweighofer *et al.*, 1998, II], all neurons have coordinates placing them at different positions within their cerebellar layer. Here, all Purkinje cells and interneurons have synapses to a subset of all granule cells with no regard to their position within the molecular/granular layer.

- No DCN and thus no MF collaterals innervating the DCN or the output of the network.

- Golgi cells are assumed to have only long term effect, regulating the activity of the granule cells in the network. This is included into the model by varying the resting potentials of all granule cells and also the synaptic strength of the mossy fiber input instead of explicit Golgi cell models.
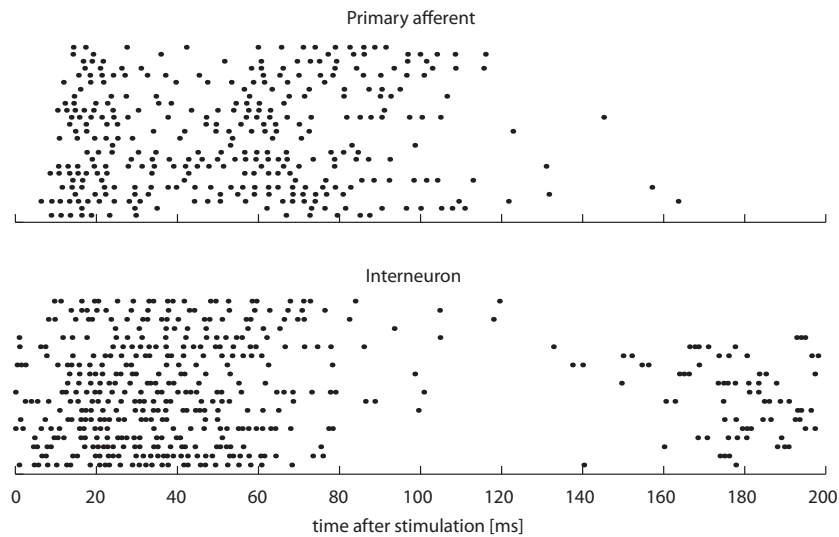
## 4.1 Neuron models



**Figure 4.1**   The primary afferent and interneuron spike trains used as input to calibrate the models

A variety of the neuron models described in chapter 2 are used to model the different neuron types introduced in chapter 3. The purpose of not using a single model for all neurons is to enable the chosen model to emulate the interesting behaviour of the different neurons, which varies both due to their location within the network, and their bio-physical nature.

When a model is chosen, some parameters are fairly well established; such as the membrane capacitance and conductance, and also the time constants of synaptic differential equations. Other parameters have to be calibrated against a known behaviour, where standardized afferent input is fed to the periphery of the network. Recorded spike trains from primary afferents and interneurons can be seen in Fig. 4.1 after mechanical stimuli has been applied to tactile skin sensors. These spike trains are used as input to test the neuron models and compare them to experimental data during the same stimulation.

As the tactile stimulation and the behaviour of the primary afferents is highly stochastic, there is no extra gain from recreating the exact behaviour found in the experimental data. Instead, either the simulated result should exhibit the same qualitative behaviour, or an average spike intensity histogram over several runs can be created, where the simulated result should be very close the actual behaviour.

### Cuneate neurons

The cuneate neurons have the most complex firing pattern of the cerebellar cells. They can both exhibit bursting behaviour, but some cuneate cells will never or seldom burst. As most of them also exhibit activity during rest, an escape rate model would

be preferred over a deterministic model. Hence, the first step of selecting a model for the cuneate neurons is to investigate whether or not a escape rate model is a viable choice; is there enough data to fit all distribution parameters, and can a typical cuneate neuron behaviour be found among the experimental data, or would it require several different models?

If the escape rate model cannot be used, the second choice is to use the EIFB model. It too requires some extra attention, as it is much more complex than the EIF model. Suitable values to the parameters from both the extra calcium channel and the potassium channel have to be chosen to make the model behave as a regular cuneate neuron.

As it is the complex bursting behaviour that make the cuneate cells interesting, the model is validated by comparing the simulated result to experimental result, without averaging over several runs.

**Granule cells**

**Table 4.1** Setup used to calibrate and validate the granule EIF model

| Type | # | Model | Input | Output |
| --- | --- | --- | --- | --- |
| Cuneate | 4 | EIFB or ER | Recorded spiketrains from 4 primary afferents and 8 interneurons | 1 granule cell |
| Granule | 1 | EIF | 4 mossy fibers | |

As the granule cells acts as noise gates with a firing threshold that is high above the neurons resting potential, they can be seen to act in a completely deterministic manner. That makes EIF the most suitable model to use.

Table 4.1 summarizes the simple network that is used to calibrate and validate the model. Four cuneate neuron models, constructed according to the previous step, are connected to the granule cell EIF model. If the cuneate cells are modeled with completely deterministic models, either their input or parameters have to be chosen so that they do not fire completely synchronized, since that would invalidate the calibration of the granule model.

Other than the calibration of a single granule cell, the setup does also allow for investigating some of the feature extracting capabilities of the cerebellar granule layer. By feeding the cuneate cells with a monotonically increasing bias current, its influence on the firing rate of the granule cells can be determined. Using different configurations of the granule models, e.g. changing the resting potential or the synaptic weights of the incoming MFs, the possibility of granular layer basis functions, used by the PC to approximate non-linear functions, could be investigated.

**Molecular layer interneurons**

Because of their high spontaneous activity, ER models should be able capture the behaviour of the interneurons better than deterministic models. Using different patterns of inhibitory connections between the interneurons, the behaviour in Fig. 3.4 on page 20 should also be recreated. As it requires that some of the neurons exhibit a slower and lingering response to the stimulation, the neurons are divided into two groups, (*1*) deep neurons with a slow response and (*2*) superficial neurons with a faster response , inspired by the molecular layer anatomy. The behaviour from Fig. 3.4 should appear in some of the superficial neurons that are inhibited by the deep

**Table 4.2**   Setup used to calibrate and validate the molecular layer interneuron escape-rate models

| Type | # | Model | Input | Output |
|------|---|-------|-------|--------|
| Cuneate | 8 | EIFB or ER | Recorded spiketrains from 4 primary afferents and 8 interneurons | $\sim$ 5 granule cells |
| Granule | 10 | EIF | 4 mossy fibers | 10 interneurons |
| Interneuron | 10 | ER | 2-3 other interneurons and 10 granule cells | 2-3 other interneurons |

neurons, causing the period without spikes at around 100 ms past the stimulation onset.

The speed of the response is modeled by changing the EPSP of the PF synapses onto the interneurons. This is not corroborated by experimental results, which instead indicate similar time constants at all PF interneuron synapses [Jörntell *et al.*, 2010]. The best solution would be to use different ISI PDFs for the deep and superficial neurons, but modifying the EPSP time constants should yield a similar result.

The network setup in table 4.2 shows the basic structure, but leaves the actual connection pattern between the interneurons to be decided through the actual simulation results. The four different connection paths that can be used between the interneurons are (*1*) from deep to superficial (*2*) from superficial to deep (*3*) between two superficial and (*4*) between two deep. The behaviour within the interneuron population can be be investigated using different patterns of these connections, ultimately looking for the behaviour shown in Fig. 3.4.

**Purkinje cells**

Escape rate models are suitable to model Purkinje cells due to their high spontaneous activity. The network structure in table 4.3 is similar to that used for the interneurons, with an added Purkinje cell model receiving synaptic input from 10 parallel fibers and 5 interneurons.

**Table 4.3**   Setup used to calibrate and validate the Purkinjecell escape rate models

| Type | # | Model | Input | Output |
|------|---|-------|-------|--------|
| Cuneate | 8 | EIFB or ER | Recorded spiketrains from 4 primary afferents and 8 interneurons | $\sim$ 5 granule cells |
| Granule | 10 | EIF | 4 mossy fibers | 1 Purkinje cell and 10 interneurons |
| Interneuron | 10 | ER | 2-3 other interneurons and 10 granule cells | $\sim$ 0.5 Purkinje cells and 2-3 other interneurons |
| Purkinje cell | 1 | ER | 5 interneurons and 10 granule cells | |

## 4.2 Complete network setup

To reach the objective of being able to investigate how several neurons in the cerebellar network behave in concert, a much larger network than the previous presented has to be constructed. The size of the network is limited by available hardware and time, but should still be large enough to emulate the behaviour that is due to the large amount of neurons present within the cerebellum. The network size used in [Schweighofer *et al.*, 1998, II] allowed the network to be trained, leading to clear improvements of the controlled arm model. Constructing the network to be of approximately that size, should at least allow it to be trained, and perhaps show other interesting properties as well.
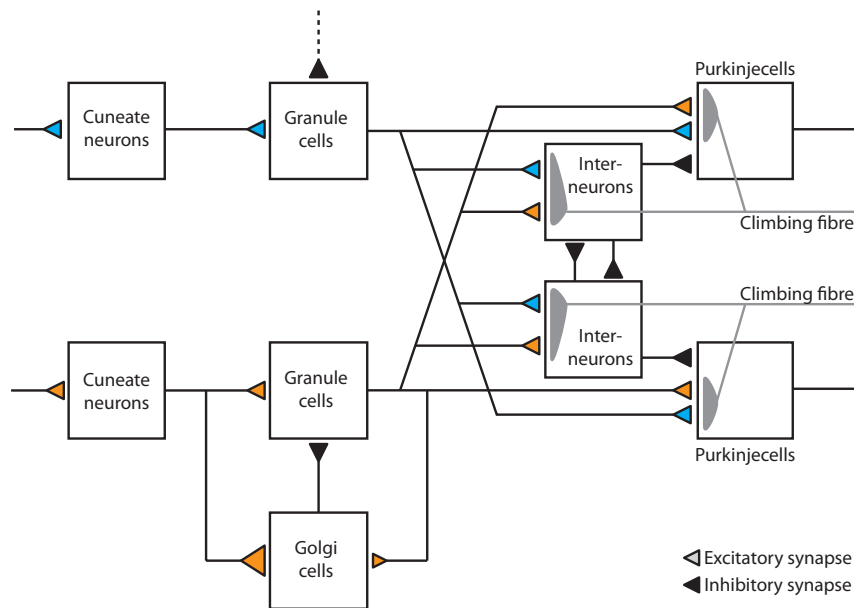


**Figure 4.2** Illustration of how the cerebellar microzone structure can be interpreted. In the constructed network, the Golgi cells are modeled implicitly through their long term effect upon the synaptic weights in the glomureli.

The actual setup used is presented in table 4.4, where the amount of neurons and their connections are shown. The actual pattern of connections does, however, still need to be established. Fig. 4.2 illustrates how information channels carrying different modalities are constructed, and does not converge until the PF create synapses upon the Purkinje cells or molecular layer interneurons. Just like real afferent input, each modality has both a positive and a negative channel, emulating proprioceptive and tactile sensory feedback from agonist/antagonist sensors. As a result of this simplification, the modalities do not cross paths either in the cuneate nucleus or in the granule layer.

In the real system, afferent input could contain state information that is not deducible from the trajectory reference, but since no muscle model or any biologically plausible tactile or proprioceptive sensors are used in the simulation, there is no motivation for afferent input to the network.

The network is further simplified by connecting each interneuron to Purkinje cells from only one microzone, further enhancing their role as sign changers in the hypothesized adaptive network shown in Fig. 3.6 on page 23.

The results from the interneuron simulations could then be used to construct the connection pattern between the interneurons, and the result from the granule cell ex-

periment could be used to calibrate the distribution of the granule cell rest potential and the MF synapses. Each Purkinje cell receives input from 720 parallel fibers and 4 interneurons chosen at random from the entire set of parallel fibers and interneurons. The interneurons do in turn receive input from 100 granule cells also chosen at random.

Since the input to the 4 groups of Purkinje cells are chosen at random from the set of all granule cells and thus all input channels, all the groups will behave equivalent in the untrained network. By connecting climbing fibers to the Purkinje cells and their respective interneurons, changing the PF synaptic weights, the Purkinje cell groups should start to converge. Since each group also has a antagonist group, Purkinje cells from those two groups could be compared to see if the training is successful. If this is the case, they should start to exhibit opposite reactions to input, where the antagonist output is at its largest when the agonist output reaches its minimum.

As the network is used to control the double joint arm described in the next section, it recieves both a positive and negative version of the angular acceleration, angular velocity and the joint angle for both the joints in the arm. In total the network receives 12 input channels, divided over 240 MFs. The output of the network is generated by four groups of Purkinje cells with 9 cells in each group. They generate both agonist and antagonist joint torque signals for both joints. The continuous output signals, $\tau_s^{CB+}$, $\tau_s^{CB-}$, $\tau_e^{CB+}$ and $\tau_e^{CB-}$, are computed by counting all spikes from the respective 9 Purkinje cells during the previous 5 ms.

**Table 4.4**   The complete network

| Type | # | Model | Input | Output |
|------|---|-------|-------|--------|
| Mossy fiber | 240 | EIF | $\pm\ddot{\theta}_s^{\text{ref}}$, $\pm\dot{\theta}_s^{\text{ref}}$, $\pm\theta_s^{\text{ref}}$, $\pm\ddot{\theta}_e^{\text{ref}}$, $\pm\dot{\theta}_e^{\text{ref}}$ and $\pm\theta_e^{\text{ref}}$ | $\sim 1.1 \cdot 10^4$ granule cells |
| Granule | 2916 | EIF | 4 mossy fibers | $\sim 5.5$ interneurons and $\sim 9$ Purkinje cells |
| Interneuron | 162 | ER | 100 parallel fibers and 2-3 other interneurons | $\sim 0.8$ Purkinje cells and 2-3 other interneurons |
| Purkinje cell | 36 | ER | 720 parallel fibers and 4 interneurons | $\tau_s^{CB+}$, $\tau_s^{CB-}$, $\tau_e^{CB+}$ and $\tau_e^{CB-}$ |

.

## 4.3  Double joint plant

The planar double joint plant used as the controlled system is illustrated in Fig. 4.3 and is completely described by Eq. (4.1). The equation shows the inverse dynamics form, which is the form that the cerebellar network should learn to approximate. The model is also used in [Schweighofer *et al.*, 1998, I], with the same parameters as those used in [Katayama and Kawato, 1993].

$$
\begin{aligned}
\tau_s ={}& \left(I_1 + I_2 + 2M_2 L_1 L_{g2} \cos\left(\theta_e\right) + M_2 L_1^2\right) \ddot{\theta}_s \\
&+ \left(I_2 + m_2 L_1 L_{g2} \sin\left(\theta_e\right)\right) \ddot{\theta}_e \\
&- M_2 L_1 L_{g2} \sin\left(\theta_e\right) \dot{\theta}_e^2 - 2 M_2 L_1 L_{g2} \sin\left(\theta_e\right) \dot{\theta}_e \dot{\theta}_s \\
\tau_e ={}& I_2 \ddot{\theta}_e + \left(I_2 + M_2 L_1 L_{g2} \cos\left(\theta_e\right)\right) \ddot{\theta}_s + M_2 L_1 L_{g2} \sin\left(\theta_e\right) \dot{\theta}_s^2
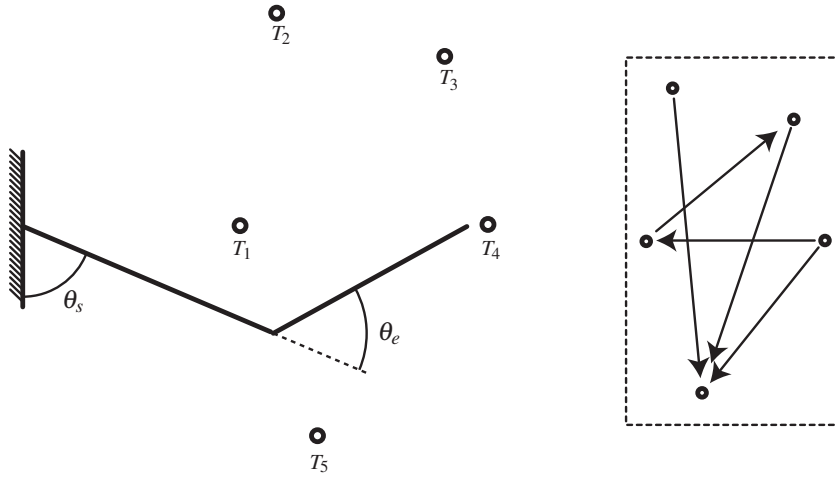\end{aligned}
\tag{4.1}
$$

**Figure 4.3**   The planar double pendulum in mixed coordinates used to model the human arm. The points $T_1$ to $T_5$ are used as start and stop coordinates for the motions used during the simulation. The five motions used can be seen within the dashed rectangle to the right.

The difference compared to the setup in [Schweighofer *et al.*, 1998, I] is the absence of a muscle model. Since the network acts in joint space, the transformation to torque space in the setup by Schweighofer is attributed to a region in the CNS called C3/C4. By assuming that the transformation from joint to torque space in that region is perfect, implementing an exact inverse model of the muscle dynamics, the muscle model and inverse muscle model cancel out, allowing for the complete removal of the muscle model.

This simplifies the simulation setup, and since the objective of the thesis work does not contain a detailed description or investigation of the muscle model, it is a feasible simplification. Even without the muscle model, the network has to learn the inverse dynamics of the arm, and despite that the human arm is much more complex, with more actuators, sensors and degrees of freedom, the result will be a trained network, and its properties can be investigated.

The motions used to train the network originates from [Koike and Kawato, 1995], and the trajectories are miminum jerk trajectories generated in joint space as opposed to the trajectories used in [Schweighofer *et al.*, 1998, I] which are in task space. This leads to slightly more curved trajectories. The start and end point of all motions can be seen in Fig. 4.3, labelled $T_1$ to $T_5$.

## 4.4  Controller structure

Other than the network, the arm is also controlled by an ordinary PD-controller and one additional simple feed-forward controller. The entire setup can be seen in Fig. 4.4. The arm is controlled through the torque to the shoulder joint, $\tau_s$ and the torque to the elbow joint, $\tau_e$, which are calculated as the sum of the control signals from the three controllers according to Eq. (4.3).

The feed-forward controller is a simplification of the inverse dynamics in Eq. (4.1), leading to Eq. (4.2). The same structure is also used in [Schweighofer *et al.*, 1998, I].
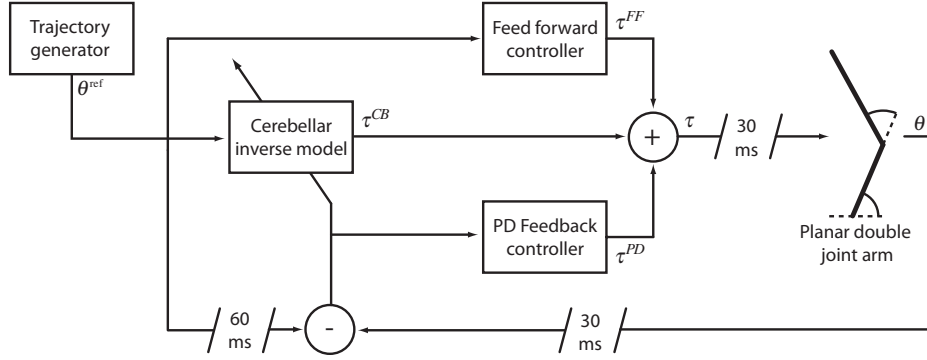
**Figure 4.4** The controller structure of the simulation setup

$$\begin{pmatrix} \tau_s^{FF} \\ \tau_e^{FF} \end{pmatrix} = \begin{pmatrix} \alpha_{FF} + \beta_{FF}\theta_e & 0 \\ 0 & \lambda_{FF} \end{pmatrix} \begin{pmatrix} \ddot{\theta}_s^{\text{ref}} \\ \ddot{\theta}_e^{\text{ref}} \end{pmatrix} \tag{4.2}$$

$$\begin{aligned} \tau_s &= \tau_s^{FF} + \tau_s^{PD} + \tau_s^{CB+} - \tau_s^{CB-} \\ \tau_e &= \tau_e^{FF} + \tau_e^{PD} + \tau_e^{CB+} - \tau_e^{CB-} \end{aligned} \tag{4.3}$$

## 4.5 Plasticity model

The plasticity model used to train the complete network borrows its main features from the setup in [Schweighofer *et al.*, 1996]. The similarities allow for comparisons, but the model also contains some serious flaws. The most important being that it cannot explain the bidirectional timing properties between PF and CF inputs found in [Sarkisov and Wang, 2008].

**Weight update rule**

The basis for many neural plasticity models uses what is called Hebbian theory to update the synaptic weights in relation to their recent activity. The rules were first introduced by Donald Hebb in [Hebb, 1949], hence the name. The theory states that synapses between cells that fire simultaneously are strengthened. In the case of parallel fiber synapses upon Purkinje cells, the opposite is true, which is corrected through the inserted negation in the original learning rule, leading to

$$\frac{d\bar{g}_i^{syn}}{dt} = -\lambda \, \psi_i(t) \left( r_{CF}^{syn}(t) - \theta_M(t) \right) \tag{4.4}$$

where $\lambda$ is a learning coefficient, $\psi_i$ is described later, but depends on the activity of the PF synapse, $r_{CF}^{syn}$ is the synaptic activity from the climbing fiber, and $\theta_M$ sets the threshold between LTP and LTD of the synapse.

The threshold $\theta_M$ is added as an implicit normalization of the synaptic weights. In [Schweighofer *et al.*, 1996], an explicit weight normalization is applied at each step, increasing all weights so that the sum of all weights stay constant. Since both LTP and LTD are connected to the activity of the incoming PF, using a explicit approach

to normalizing the weights is not biologically plausible. It is however necessary to include some kind of normalization rule to keep all weight from reaching zero, or being to large, saturating the Purkinje cell.

The type of Hebbian learning rule using a threshold to regulate the balance between potentiation and depression is called a BCM rule after the authors of [Bienenstock *et al.*, 1982]. Usually, the rule inludes a quadratic $r_{CF}^{syn}$ term, and consequently $\theta_M$ should be the moving average of $(r_{CF}^{syn})^2$. To keep the linear normalization from the Schweighofer article, this is not the case here. Instead, $\theta_M$ is the moving average of $r_{CF}^{syn}$ leading to

$$\tau_M \frac{d\theta_M}{dt} = r_{CF}^{syn}(t) - \theta_M \tag{4.5}$$

By having a large enough time constant $\tau_M$, the threshold $\theta_M$ will stay close to the time average of the CF synaptic activity, without large fluctuations when the CF is activated. This will give close to the same result as a normalization rule that keeps the sum of all synaptic weights constant as the ratio between LTP and LTD regulated by Eq. (4.4) will strive to be 1 .

**Error signal**

The error signal that drives the activity of the climbing fibers contain the acceleration, velocity and angular error according to

$$e = \alpha_e \left(\theta - \theta^{\text{ref}}\right) + \beta_e \left(\dot{\theta} - \dot{\theta}^{\text{ref}}\right) + \gamma_e \left(\ddot{\theta} - \ddot{\theta}^{\text{ref}}\right) \tag{4.6}$$

where $\alpha_e$, $\beta_e$ and $\gamma_e$ are coefficients that can be used to stabilize learning rate. Since the errors are simply added, this resembles the feedback error of the control loop. Because of this it is called Feedback Error Learning (FEL) and allows for training of the model without access to the errors in joint space, using the actual feedback error[Gomi and Kawato, 1990]. Motivation for the bio-physical validity of FEL can be found in [Kawato and Gomi, 1992].

The slow firing rate of the climbing fibers can be modeled by an ER model, which uses the error signal instead of membrane potential to calculate the current distribution of ISI. Using the same sigmoid function as in the original ER models, two equations like that shown in Eq. (4.7) can be used to describe the mean firing rate and inverse ISI standard deviation.

$$I_{CF}(e) = p_{1e} + \frac{p_{2e}}{1 + \exp\left(p_{3e} - e\right)/p_{4e}} \tag{4.7}$$

The error signal delays, caused by muscle reaction times and neural transmission delays, are counteracted by the introduction of an additional second order state, $\psi$. The method is also used in [Schweighofer *et al.*, 1998, II] and originates from [Schweighofer *et al.*, 1996]. Eq. (4.8) contain the definition of $\psi$, which can be seen as an autoregressive process with the synaptic activity as input. It works by delaying the plasticity caused by the synaptic input, synchronizing the time it takes for the state to reach its maximum with the delay of the error signal. This creates an eligibility window, open for a short period after the synapse receives input spikes, during which plasticity is possible. The dynamics and timing of the window is controlled by the parameters $\alpha_\psi$, $\beta_\psi$, $\gamma_\psi$ and they should be chosen so that Eq. (4.8) reaches it peak after 60 ms, which is the combined delay from the control loop in Fig. 4.4.

$$\alpha_\psi \frac{d^2\psi_i}{dt^2} + \beta_\psi \frac{d\psi_i}{dt} + \gamma_\psi \psi_i = r_i^{syn} \tag{4.8}$$

The eligibility window approach does not take the bi-directional timing found in experimental studies into account. Neither does it explain how the eligibility window is synchronized with the error signal in the first place. These two flaws in the model need to be addressed to create a detailed biologically plausible model for plasticity caused by climbing fiber activity, but that work is beyond the scope of this thesis.
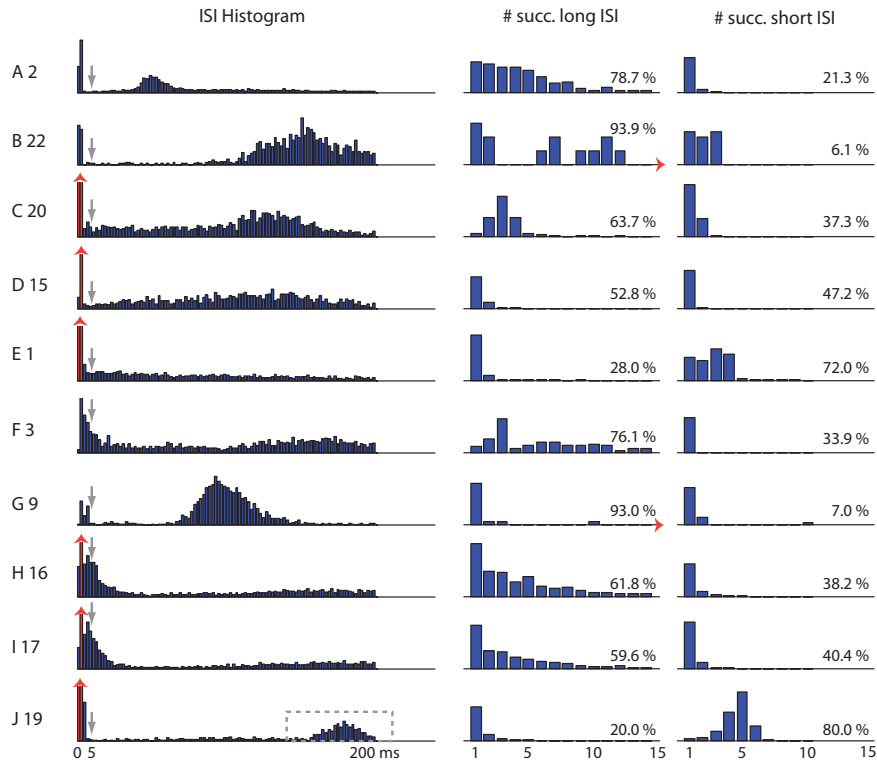
# 5. Results

## 5.1 Cuneate neurons



**Figure 5.1** Properties of ten different cuneate neurons under no external input displayed in histograms showing the distribution of their ISIs (left), the likelihood of successive long ISIs (middle) and the likelihood of successive short ISIs (right). The percentages show the total distribution between long and short ISIs, the red arrowheads denote significant overflows in the figure and the gray arrows show where the border between short and long ISIs is (5 ms). The dashed box (neuron J) show a rebound peak, which is completely made up of ISIs following a short ISI.

Spontaneous activity from 30 different cuneate neurons registered *in vivo* was analyzed to decide whether it would be possible to build a bursting ER model. The found behaviour of the different neurons, shown in Fig. 5.1 using ten of them, does exhibit some common characteristics, but is in general to diverse to allow the construction of a generic bursting ER model. It would be possible to construct several different models, but since all the models are also required to work under non-stationary conditions, each model would require data from the same cuneate neuron at several different membrane potentials. This would require an enormous amount of data that is currently not available. Further analysis is also needed to describe how the state transition probabilities of the underlying HMMs change depending on the neuronŠs membrane potential.

Looking further at the dynamics of responses to different input, such as bias current steps, it is clear that the transient behaviour following input is very interesting.
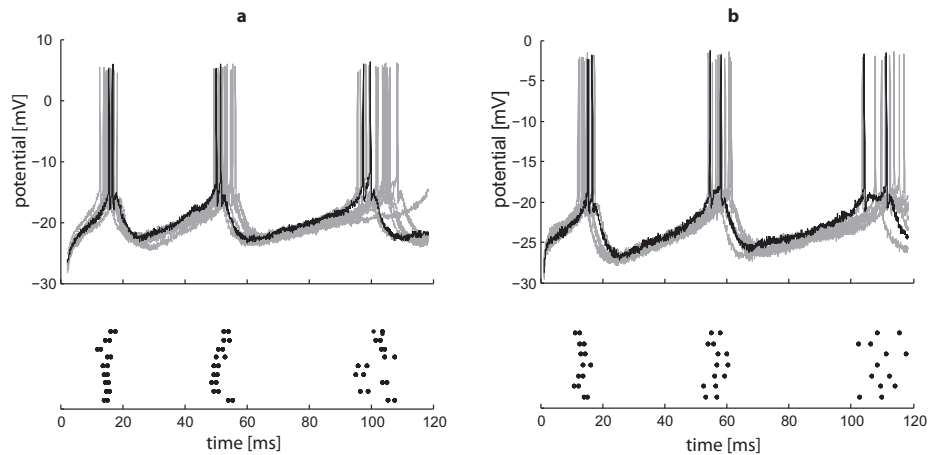
**Figure 5.2** A cunate neurons response to bias current steps. **a)** The depolarizing current step followed after a long period of hyperpolarization (800 ms). **b)** The depolarizing current step followed a short period of hyperpolarization (150 ms).

Approaching the model from the steady-state behaviour might lead to a loss of important dynamic properties of the bursting neuron. While the spontaneous behaviour and the response to sensory stimulus is highly stochastic, the responses to controlled input steps follow a strict pattern shown in Fig. 5.2. It might be that the responses from the cuneate neuron is not that stochastic, but that the mechanical sensory stimulus and the neural pathways leading to the cuneate neuron are the primary causes of the stochastic behaviour. As the cuneate neurons have resting potentials very close to their firing thresholds, it could also be caused by the stochastic components of the inhibitory input from cuneate interneurons. The spontaneous input from cuneate interneurons can be seen in Fig. 4.1 on page 26 after 160 ms have passed since the onset of the stimulation.
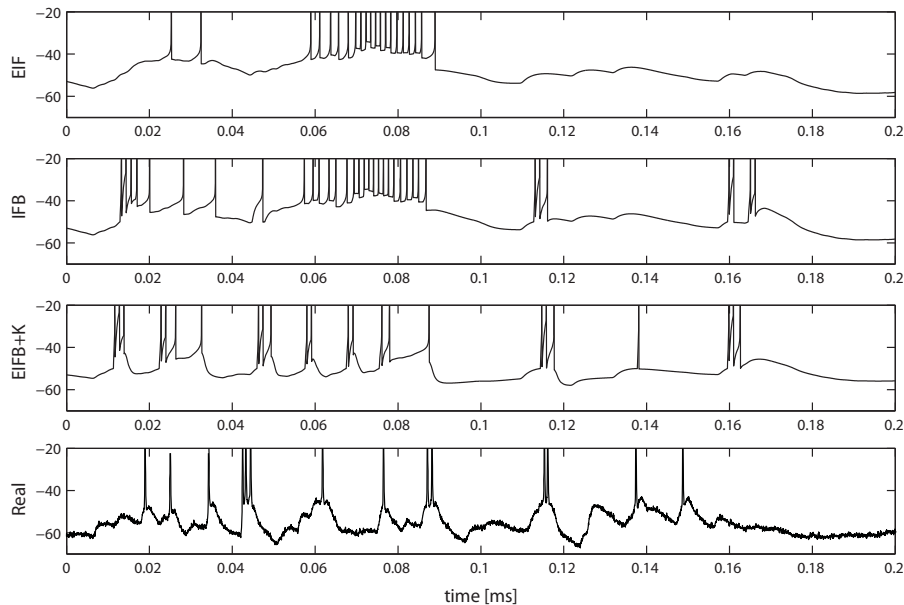


**Figure 5.3** Evolution of the different simulation models for cuneate neurons, showing their difference simulated with primary afferent and interneuron input from *in vivo* data.

Using the assumption of a deterministic behaviour, or at least that the stochastic

behaviour of the cuneate neuron does not influence the important dynamics, the EIFB model can be used. This model does however fail to explain the neuronŠ spontaneous activity. Fig. 5.3 contains simulation results from the used EIFB model, including results from a real registration *in vivo*.
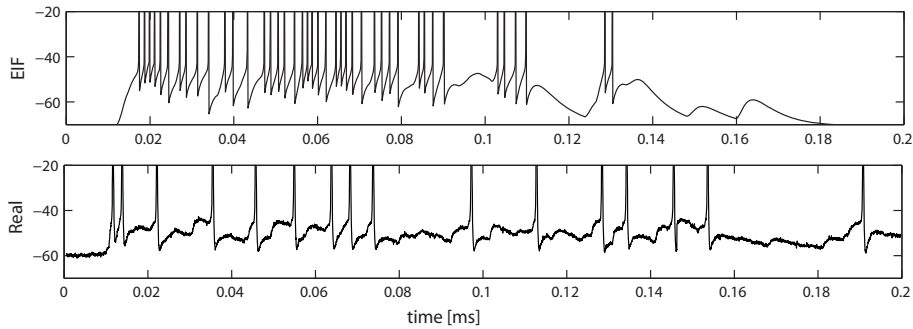
## 5.2  Granule cells



**Figure 5.4**   Comparing the output of the EIF-model with real *in vivo* measurements from a granule cell.

Fig. 5.4 show the simulation results of the constructed EIF model and *in vivo* measurements of a granule neuron. The shape of the action potentials and the EPSPs have a similar appearance, while the overall activity of the model is much higher. This is due to slightly higher synaptic weights and in addition to that the *in vivo* measurement was made during a much lighter stimulation than that used to create the spiketrains used as input to the simulations. Notice how the membrane potential is reset to a level 10-15 mV below the equilibrium.

## 5.3  Interneurons

ISIs registered *in vivo* from one interneuron at five different membrane potentials were used to create PDFs describing the spike rate. The different membrane potentials were induced by applying a bias current through the membrane of the neuron. Histograms of the ISI distributions at the different membrane potentials can be seen in Fig. 5.5 together with the fitted log-normal PDFs.

The sigmoid curve described in Eq. (2.15) on page 13 was then fitted to the mean and standard deviation of the found PDFs. Fig. 5.6 shows the different relationships, where the ISI mean and standard deviation can be found in the top graph, the sigmoid curve in the middle graph, and the mean and standard deviation of the underlying normal distributions in the bottom graph.

Different connection patterns between five superficial and five deep interneurons were investigated, with the result found in Fig. 5.7. Using a random pattern of connections where all the interneurons received inhibitory connections from three random other interneurons, the superficial neurons showed no signs of the sought after quiet period. In Fig. 5.7 **b** the connection pattern was segmented between the superficial and deep neurons, resulting in a quiet period resembling the one found in the experimental data.
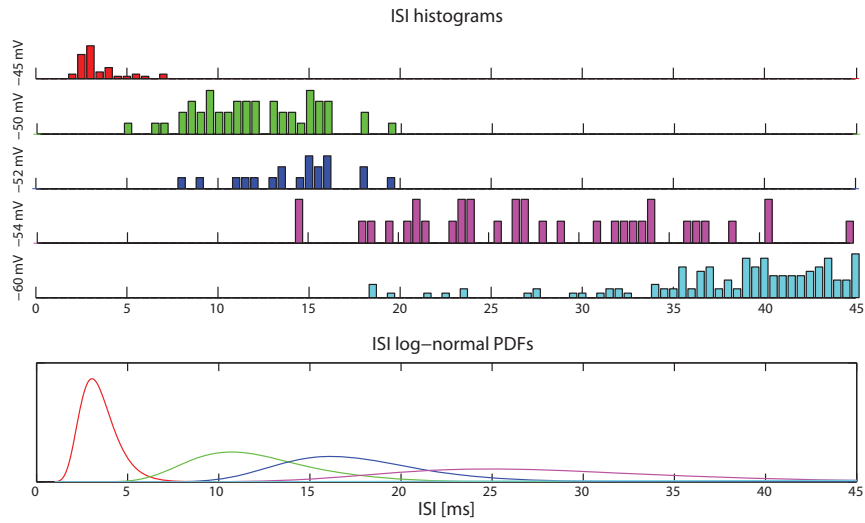
**Figure 5.5**   Interneuron ISI histograms at five different membrane potentials and below them the corresponding log-normal PDFs. Note that the most of ISIs recorded at -60 mV were longer than 45 ms, which explains why the corresponding PDF is almost negligible between 0 and 45 ms.
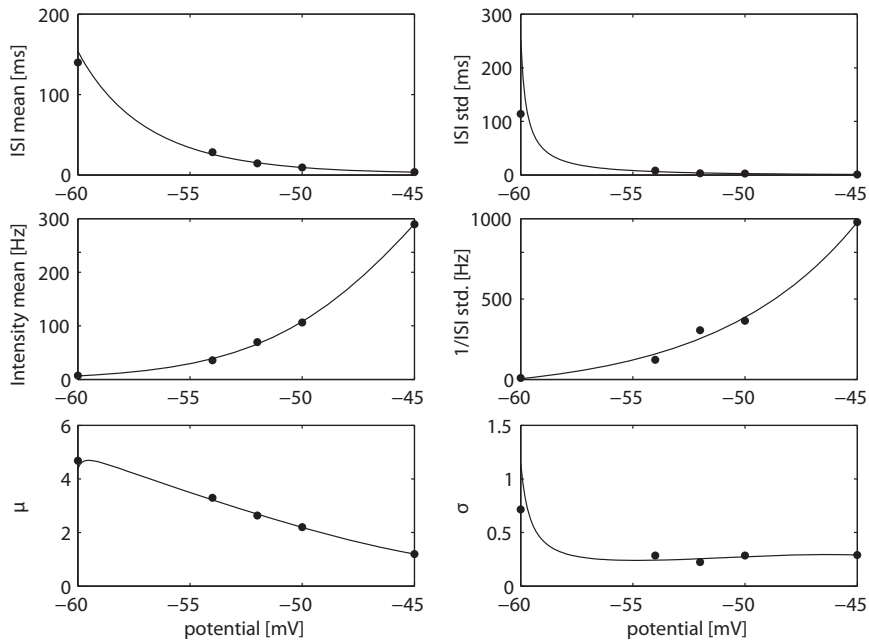


**Figure 5.6**   Logistic function fitted to the mean and std dev. of the spike rate of a interneuron at five different membrane potentials. The corresponding histograms and distributions are shown in Fig. 5.5.

During the simulation yielding the result in figure **b**, each superficial interneurons received three connections from randomly selected deep interneurons, while the deep neurons received two connections from superficial interneurons and one from another deep interneuron.
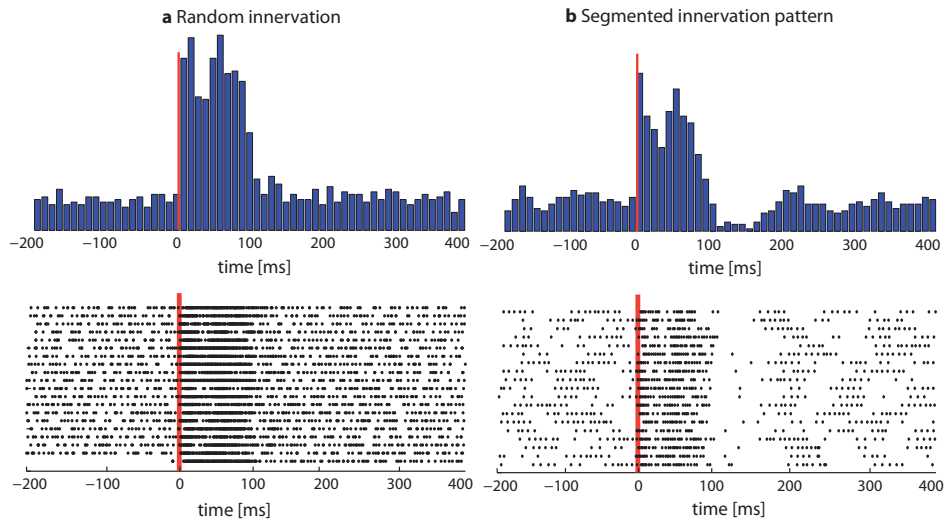


**Figure 5.7** Comparing two simulation results with different connection patterns. Both show the behaviour of interneurons with fast EPSP time constants. **a)** generated with all interneurons receiving three completely random inhibitory connections, as opposed to **b)** where the three connections were chosen depending on the speed of the interneuron EPSP time constants. The red line marks the tactile stimulation onset.
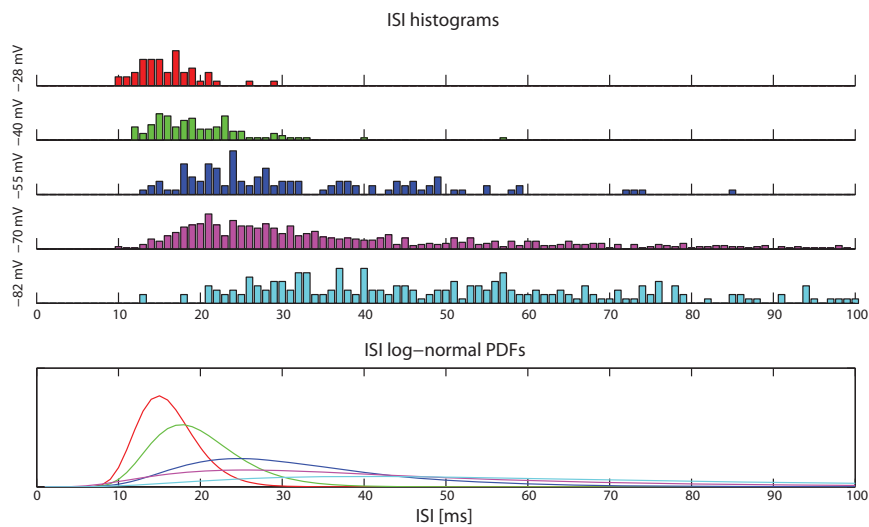
# 5.4 Purkinje cells



**Figure 5.8** Purkinje cell ISI histograms at five different membrane potentials and below them the corresponding log-normal PDFs.

The Purkinje cell ER model was constructed using the same procedure that was used modeling the interneurons. The ISI histograms and fitted log-normal PDFs at five different membrane potentials can be found in Fig. 5.8, and the fitted sigmoid curves in Fig. 5.9. Fig. 5.10 shows the simulation result, displayed as spiketrains and a histogram summing them up, compared to spike trains from a Purkinje cell registered *in vivo*.
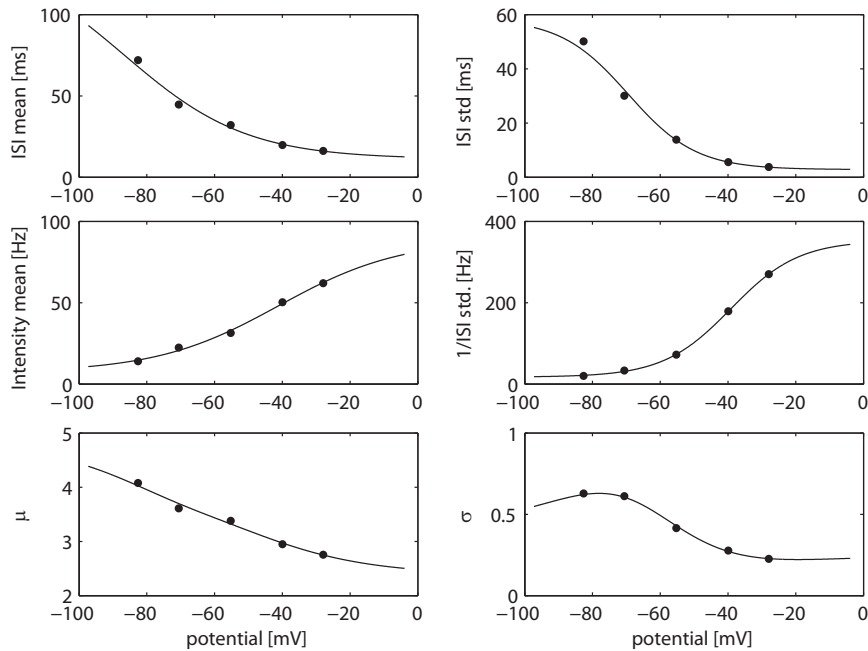


**Figure 5.9**   Sigmoid function fitted to the mean and std dev. of the spike rate of a Purkinje cell at 5 different membrane potentials.The corresponding histograms and distributions are shown in Fig. 5.8.
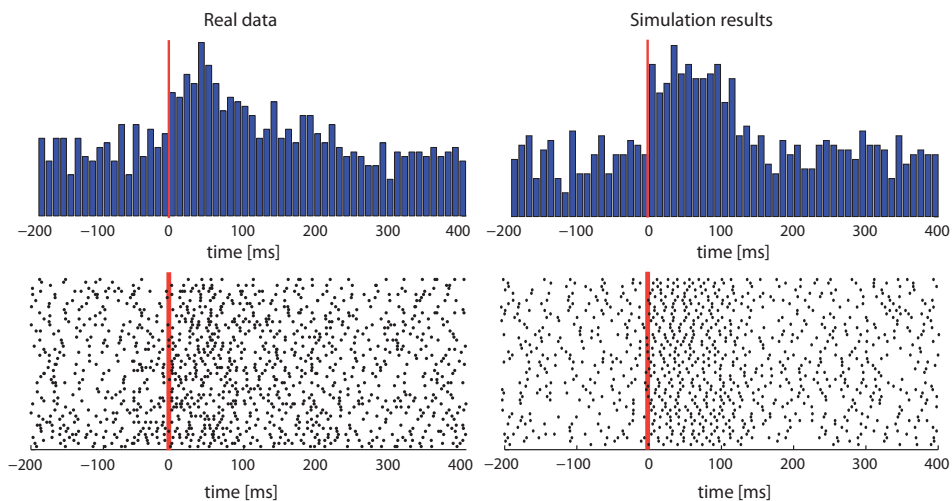


**Figure 5.10**   Comparing real Purkinje cell spiketrains with those generated by the ER model. The red line marks the tactile stimulation onset.
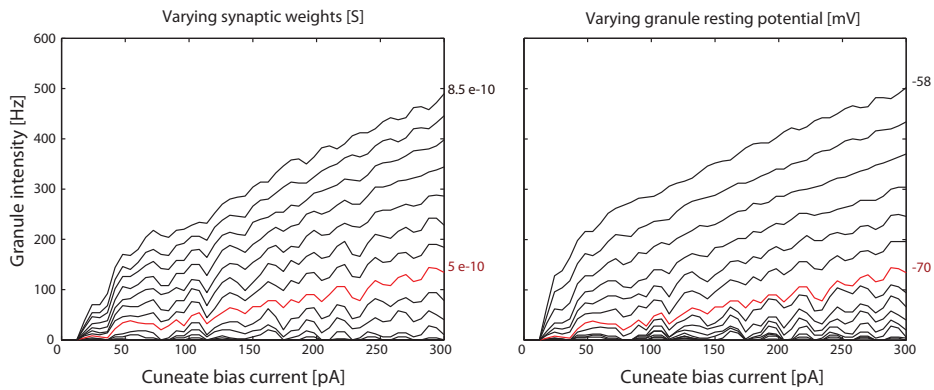
## 5.5 Granular basis functions



**Figure 5.11** Simulation results from a small network with four cuneate neurons connected to one granule cell. The red curves in both the figures are have the same synaptic weight and resting potential setup.
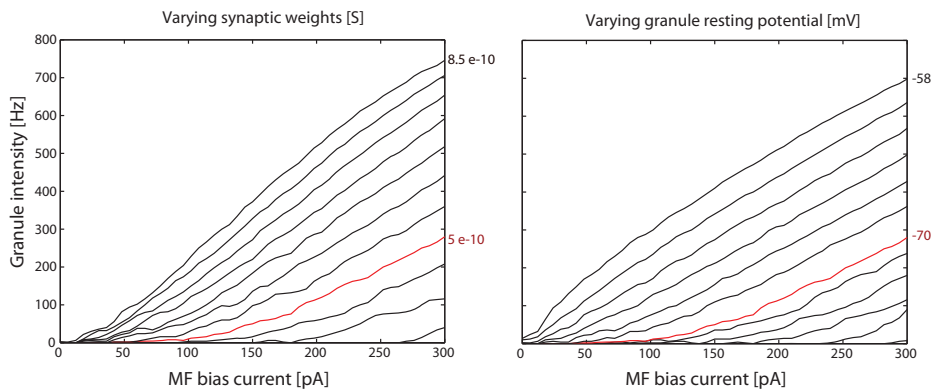


**Figure 5.12** Simulation results from a small network with four non-bursting mossy fibers connected to one granule cell. The red curves in both the figures are have the same synaptic weight and resting potential setup.

The setup used to construct and validate the granule cell EIF model was also used to investigate the basis function properties of the junctions between the incoming MFs and the granule cells. The results can be seen in Fig. 5.11, where the MFs were modelled as bursting cuneate neurons, and in Fig. 5.12, where the MF were modelled as non-bursting neurons. The influence of Golgi cells was assumed to be static, only affecting the distribution of the synaptic weights between the MFs and the granule cells. Additionally, the influence of varying granule resting potentials was also investigated.

## 5.6 The complete network

Fig. 5.13 show the five motions the arm performed during the simulations. The end point error is improved only in the second motion, while it is clearly worsened in both motion four and five. The error signal history during 200 simulations, including
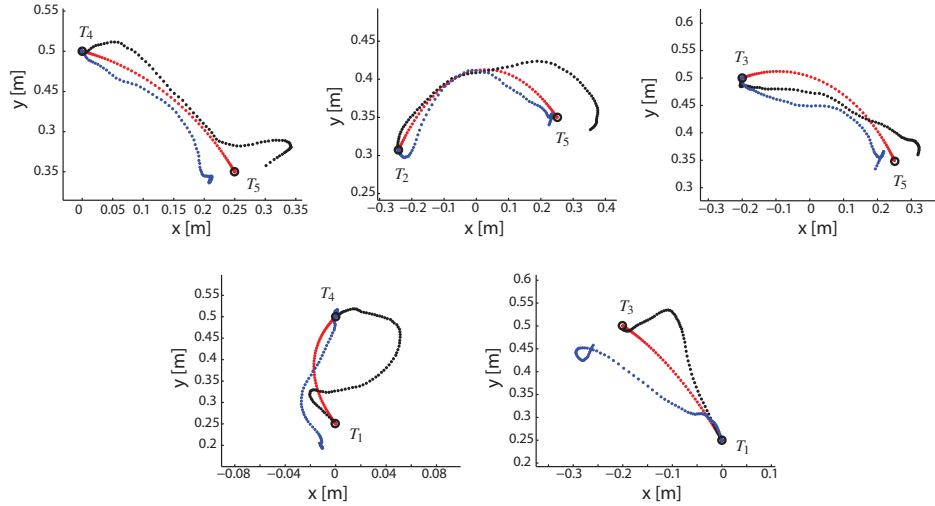
**Figure 5.13** Reference trajectories and the simulated motion of the arm model before and after 200 simulations. The reference trajectory is shown in red, the untrained arm model in black and the trained arm model in blue. The start and endpoints of the motions are marked with black circles and their labels, $T_1$ to $T_5$
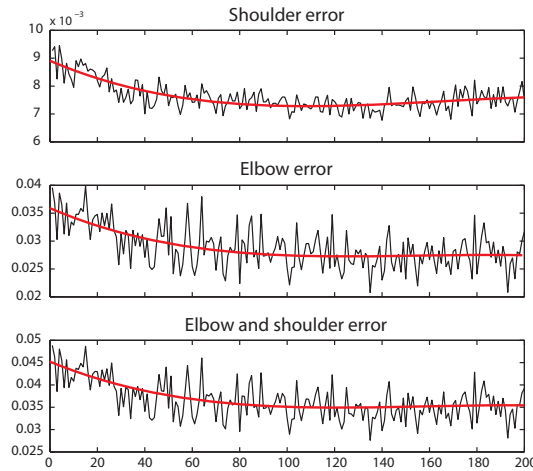


**Figure 5.14** The mean of the error $e$ at each run. The red curves illustrate the overall trend.

all five motions, can be seen in Fig. 5.14. The trend of both joint errors show clear improvements, but the shoulder error reaches its minimum after 100 simulations, after which its starts to grow again. This problem arose during all simulation trials, implying it is a inherent limitation of the current simulation setup.

Fig. 5.15 and 5.16 show the membrane potential of simulated Purkinje cells involved in shoulder and elbow control. As long as the membrane potential is within the linear region of the used intensity function, it can be seen as the control output of the network model. After 200 simulations, the activity is clearly related to the ideal inverse model torque. There are however no clear signs of any non-linear approximations using the granule basis functions in Fig. 5.12. Most of the correlation is due to high synaptic weights against signals containing acceleration references.
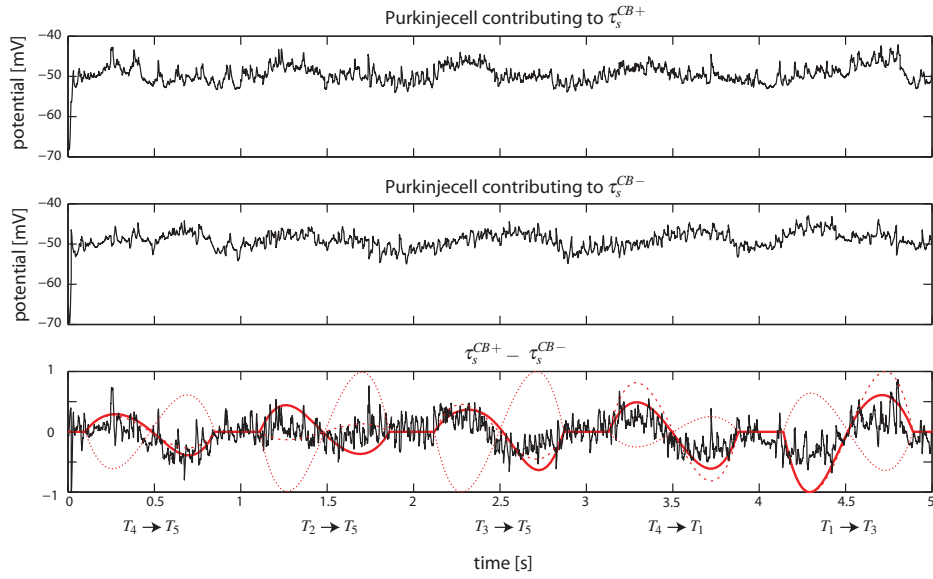
**Figure 5.15**  Membrane potential of two Purkinje cells involved in controlling the shoulder joint after 200 simulations. The Purkinje cell shown in the top graph belongs to the microzone which generates the $\tau_s^{CB+}$ signal, while the Purkinje cell shown in the middle graph belongs to the antagonist microzone generating $\tau_s^{CB-}$ signal. The bottom graph illustrates how $\tau_s^{CB+}$ and $\tau_s^{CB-}$ interacts and compares them to the ideal torque $\tau_s^{\mathrm{ref}} - \tau_s^{FF}$ (solid line), the shoulder acceleration reference $\ddot{\theta}_s^{\mathrm{ref}}$ (dotted line) and the elbow acceleration reference $\ddot{\theta}_e^{\mathrm{ref}}$ (dashed line). All components of the bottom graph are normalized so that their largest absolute value equals 1.
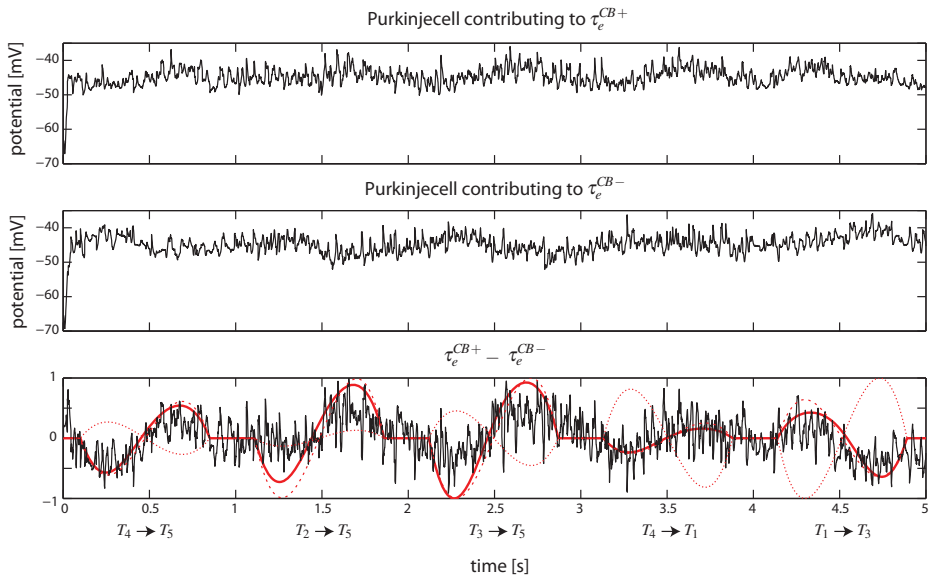


**Figure 5.16**  Membrane potential of two Purkinje cells involved in controlling the elbow joint after 200 simulations. The Purkinje cell shown in the top graph belongs to the microzone which generates the $\tau_e^{CB+}$ signal, while the Purkinje cell shown in the middle graph belongs to the antagonist microzone generating $\tau_e^{CB-}$ signal. The bottom figure illustrates how $\tau_e^{CB+}$ and $\tau_e^{CB-}$ interacts and compares them to the ideal torque $\tau_e^{\mathrm{ref}} - \tau_e^{FF}$ (solid line), the elbow acceleration reference $\ddot{\theta}_e^{\mathrm{ref}}$ (dotted line) and the shoulder acceleration reference $\ddot{\theta}_s^{\mathrm{ref}}$ (dashed line). All components of the bottom graph are normalized so that their largest absolute value equals 1.

43

# 6. Discussion

The purpose of the thesis was to continue the work of [Dürango, 2010], by extending it with models describing all neurons within the cerebellar microcircuitry, and connecting the constructed network to perform a proof-of-concept control task. During the work suitable models were found, and in the case of Golgi cells, their behaviour was modeled indirectly through the MF granule cell synapses. The work is not complete, and all the models require some further development and validation. Most of the validation data was from a single neuron only, and even though the data qualitatively represented the average case neuron behaviour, the extreme cases are equally important.

The models and the network setup were chosen using the basic, but not sole prevailing viewpoint, that the cerebellum acts as an adaptive filter. The purpose was to make it possible to decide which neuronal behaviour should be emphasized and used to select models that also exhibited the same kind of behaviour. It reduces the apparent complexity of the neuron, which could of course also lead to loss of important features. This makes further validation of the individual neuron models, and their behaviour in concert, even more important.

## 6.1 About the results

### The cuneate nucleus

The behavioural diversity among the analysed neurons does almost completely rule out the use of a ER HMM to model the behaviour of the cuneate neurons. Since the cuneate neurons seem to have a almost deterministic response when stimulated, it might also be hard to actually find states with ISIs that can be considered renewal. If further analysis manages to find relationships between the membrane potential and state transition probabilities and the ISI peak PDF shapes, the ER model is at least very good at describing spontaneuos activity. The analysis might also lead to the classification of different types of cuneate neurons, which could be of interest even if other neuron models are used.

The simulated response to the primary afferent and interneuron input to the cuneate EIFB model have a clear resemblance to measurements made *in vivo*. The biggest issue with the EIFB model is its lack of stochastic components and absence of spontaneuos activity. It can be induced by changing the resting activity either close enough to $V_t$ or above $V_{Ca}$. This will however only lead to a completely deterministic and completely regular behaviour of the spikes generated (see Fig. 2.2 on page 11), which does not resemble the ISI distributions which was found from real cuneate neurons in Fig. 5.1 on page 35.

The spontaneous activity could also be attributed to activity from cuneate interneurons which also exhibit relatively high spontaneous activity. As the cuneate neurons require very little excitatory stimulation to burst, the spontaneuous activity from the interneurons in combination with a resting potential within the spiking range of the neuron might be enough to cause the spontaneous activity of the cuneate neurons.

**Molecular layer interneurons**

The interneuron model was created using *in vivo* data from one single superficial interneuron. The number of registered ISIs from the neuron varied greatly between the different potentials, but never reached a large enough number to validate the fitted PDFs using e.g. the Kolmogorov-Smirnov test. While results in Fig. 5.5 and 5.6 on page 38 look reasonable, the use of the log-normal distribution and the renewal hyphothesis should be further investigated using measurements from several different interneurons.

The fitted curves in Fig. 5.6 are in addition to this used for extrapolation, propagating small errors of any individual PDF from Fig. 5.5 into much larger errors when the ER model operate at potentials lower than -60 mV or higher than -45mV. This could be remedied by using the minimum and maximum firing rate of the neuron, creating a strict interpolation task as those values in theory are reached at membrane potentials of negative and positive infinity respectively.

The investigated interneuron connection pattern that lead to simulation results (see Fig. 5.7 on page 39) resembling experimental data was constructed with the actual molecular layer anatomy in mind. Even though there is no clear anatomical evidence that the interneurons innervate each other, it is hard to explain the histogram in Fig. 3.4 on page 20 in any other way. The simulation results further corroborate this assumption even though it cannot be used to confirm one specific pattern.

It should also be noted that the simulation results show a binary oscillatory behaviour, which is also present in the experimental data during periods of no stimulation. It can be seen as short periods with little or no activity in the histogram and spiketrains in Fig. 3.4 between 170-200 ms and 280-330 ms. The behaviour is present during at least 30-50 % of the registered spike trains. The same type of periods with almost no activity can be found in the simulation results in Fig. 5.7. In the simulations the behaviour was caused by interaction between the entire group of superficial neurons and the entire group of deep neurons. Only one of the groups was active at a time, leading to the oscillatory behaviour where one of the groups suppressed the other.

The difference between the superficial and deep neurons was modelled by changing their EPSP speed, leading to a fast response from the superficial neurons and a slow response from the deep neurons. While this does explain the experimental results, there seems to be no such distinction between superficial and deep neurons *in vivo*. It is possible that the same effect could be reached using two ER-models, or perhaps with another connection pattern. Currently, none of the setups are corroborated by any experimental evidence.

Finally, both the histograms in Fig. 5.7 have a sharp peak at the onset of stimulation which is not present in the histogram in Fig. 3.4. This could be due to that the interneuron with the response in Fig. 3.4, receive input from several other receptive fields surrounding the primary receptive field, which is the only source during the simulations. Since all cuneate neurons receive input from the same type of primary afferents, and have no spontaneous activity, they will all be inactive and ready to react with a burst when the first primary afferent spike arrives. As can be seen in Fig. 4.1 on page 26, the primary afferent spiketrains show an extra high intensity during the first 20 ms of the stimulation. This peak, together with all cuneate models being primed an ready to fire, could be what is causing the peak in the simulation results as well.

**Purkinje cells**

The Purkinje cell model resembles the model used for the molecular layer interneurons, and suffers from the same difficulties. Just as with the interneuron model, a single Purkinje cell provided all the data used to fit the model parameters, and none of the ISI histograms in Fig. 5.8 had enough ISIs to enable any statistical methods to validate or reject of the log-normal distributions.

The simulation results do also show evidence of the same initial peak (see Fig. 5.10 on page 40), which is also present in the interneuron results. In addition to the initial peak, the simulation results fail to have the trail of slightly higher activity between 120 and 250 ms found in the experimental data. Just as the initial peak, this could be due to input from neighbouring receptive fields, that respond to the tactile event slightly before and after the main receptive field.

**Network behaviour**

The adaptive filter hypothesis assumes that some kind of signal transformation takes place before the signals reach the PFs and the PCs. There is a clear need to be able to approximate non-linear functions if the cerebellum is to be able to approximate the inverse dynamics of any of the motor systems within the body. The signal transformation properties of the simulated granular layer show some promising behaviour that can in fact be used as basis functions to approximate any continuous functions.

In Fig. 5.12 on page 41, the resulting bias to intensity relationship, when the granule model was connected to four non bursting mossy fibers closely resemble the simplified basis functions in Fig. 6.1. Fig. 6.1 does also show how such basis functions can be used to approximate a quadratic equation, but they can in theory be used to approximate any given function perfectly as long as enough different basis functions are availiable. This could of course help explain the large amount of granule cells.
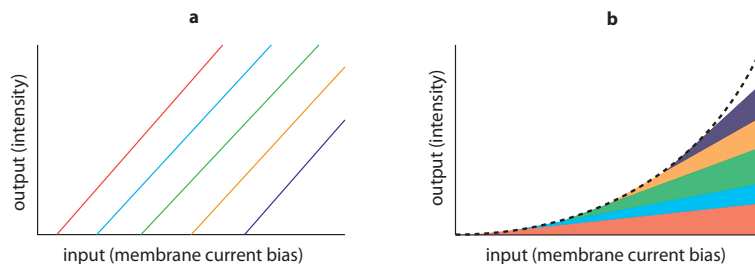


**Figure 6.1**   Sketch showing the possible use of the found granule basis functions in Fig. 5.12 on page 41. **a)** Five basis function sketches, that could be created either by varying the resting potential of the granule cells. Varying the synaptic weights would also lead to different slope angles. **b)** The five basis functions are combined with varying weights to approximate a quadratic function (dashed).

The result when the non-bursting MF were replaced by bursting cuneate cells (see Fig. 5.11) show a completely different behaviour. Instead of the linear growth found using the non-bursting neurons, the cuneate cellsŠ tendency to burst even at very small stimulations lead to an immediate high intensity of the granule cells, disregarding the synaptic weights or granule cells resting potential. The different responses indicate that bursting MFs and non-bursting MFs might be used for different purposes.

The most obvious flaw of the complete network is its learning instability. After approximately 100 trials, the error of the shoulder joint started to grow (see Fig.

5.14 on page 42). The growing error is caused by a drift of the mean activity of the opposite microzones controlling the torque joint. In one of the microzones, the mean intensity of its Purkinje cells will grow larger than the intensity of the Purkinje cells from the opposite zone. As the learning rule compensates for static errors through the $\theta_M$ sliding threshold, it will not reduce the error, but it is free to grow indefinitely. This is a inherent flaw in the learning rule, which needs to be compensated somehow in order to build a stable working adaptive model of the cerebellum.

Even though the used plasticity model has flaws leading to instability, the Purkinje cell activity in Figs. 5.15-5.16 on page 43 show clear signs of adaptation towards the ideal torque. Since the regular feed forward controller does not handle the cross-joint terms of the inverse dynamics, those should be visible in the cerebellar control signal. It means that the shoulder torque should be highly correlated with the elbow acceleration and vice versa. That effect is also clearly visible in the two figures.

The found granule basis functions would also allow the signals to approximate the non-linear relations of the inverse dynamics. As those effects are small in comparison with the acceleration correlations, and would also need motions where the non-linearities matter, they could not be expected to be distinguishable in the cerebellar control signal without using motions that purposely emphasize the nonlinear arm dynamics. Even so, there is some evidence of such a behaviour among the PC regulating the shoulder torque 5.15. During the second motion, between $T_2$ and $T_5$, the signals seems to correlate with the ideal torque rather than the elbow acceleration.

## 6.2 Future work

### Experimental setup

Even though the arm model used here was quite naive compared with the arm and muscle model in [Schweighofer *et al.*, 1998, I], it contained both nonlinearities and cross dependencies between the two degrees of freedom. While this allowed for the interesting results in Figs. 5.15-5.16, it has fundamental limitations which leaves some features of the cerebellum without explanation. Using the current setup, there is for example no need for sensory feedback into the cerebellum, since it would contain exactly the same information which is also part of the reference signals. The cerebellum do however receive an abundance of afferent tactile and proprioceptive information that seems to be actively involved in motion control (see the synaptic weight distribution in Fig. 3.3 on page 19). To investigate what role such information play, the current setup would have to be expanded with a better bio-physical model of the muscle system, including models of the proprioceptive and tactile feedback.

Some further investigation might on the other hand benefit from a simplification of the current setup. To evaluate the influence of different parts and patterns of the cerebellar microcircuitry, a simple performance metric should be designed. Instead of using a complete and detailed arm model, the inverse dynamics that the cerebellum should learn to mimic could be broken down into smaller components. This would make it much simpler to evaluate how well the trained inverse model actually approximates the non linear terms of interesting equations one at a time. The same approach could be used to investigate if and how the network deals with derivative and integrating action. The influence of different connection patterns and neurons, such as the tested interneuron patterns or the Golgi cell dynamics, could then perhaps be attributed to how well the cerebellum can approximate different types of functions and operators. Such an approach would hopefully also help to explain the content of the

CF signals, which still remain enigmatic.

**Plasticity model**

The currently used plasticity model is flawed in more than one way. The first flaw is the drift off that occurs due to the $\theta_M$ threshold, but the main problem is the lack of bio-physical corroboration with the eligibility window of the current setup. While it can be used to counter the delays in the feedback or error signal, it fails to explain the the bidirectional timing found in experiments. The current setup will only react if the PF is activated previous to the CF activation, while the real system exhibit both types of plasticity timing properties. Furthermore, the model does not explain how the timing or time constants of the eligibility windows come to be synchronized with the error signals in the first place. A complete model of the PC plasticity should take that into consideration.

The drift off due to the flawed BCM model used does also illustrate how the stability of the system is fragile in many ways that are not obvious at first glance. The cerebellum and the motor control system of the body do however seem to be very stable and robust, which is a feature that needs to be explicitly explained by the constructed models and cannot be assumed to be there.

The current model does also use the same plasticity model for both the interneuron and PC synapses. While this is a good thing if the interneurons are assumed to be simple sign changers, it is not bio-physically plausible. Having different plasticity rules might furthermore lead to other stability issues between PC inputs from interneurons and PFs that need to be considered by the constructed model.

## 6.3   Conclusion

In conclusion, the thesis left many unanswered question, and no single obvious path forward. The constructed simulation toolbox do however open up a possibility to further investigate the outlined smorgasbord of interesting topics within the cerebellar microcicuitry.

# 7. Bibliography

Abbott, L. F. (1999): "Lapicque's introduction of the integrate-and-fire model neuron (1907)." *Brain Research Bulletin*, **50:5-6**, pp. 303 – 304.

Bengtsson, F., R. Brasselet, R. S. Johansson, A. Arleo, and H. Jörntell (2011): "Optimal integration of sensory quanta in the cunate nucleus.".

Bengtsson, F. and H. Jörntell (2009): "Sensory transmission in cerebellar granule cells relies on similarly coded mossy fiber inputs." *Proceedings of the National Academy of Sciences*, **106:7**, pp. 2389–2394.

Bienenstock, E., L. Cooper, and P. Munro (1982): "Theory for the development of neuron selectivity: orientation specificity and binocular interaction in visual cortex." *The Journal of Neuroscience*, **2:1**, pp. 32–48.

D'Angelo, E. (2008): "The critical role of golgi cells in regulating spatio-temporal integration and plasticity at the cerebellum input stage." *Frontiers in Neuroscience*, **5:0**, p. 5.

Dean, P., J. Porrill, C. Ekerot, and H. Jörntell (2010): "The cerebellar microcircuit as an adaptive filter: experimental and computational evidence." *Nature Reviews Neuroscience*, **11:1**, pp. 30–43.

Dürango, J. (2010): "Analysis and simulation of cerebellar circuitry." Master's Thesis ISRN LUTFD2/TFRT--5860--SE. Department of Automatic Control, Lund University, Sweden.

Ekholm, A. and J. Hyvärinen (1970): "A pseudo-markov model for series of neuronal spike events." *Biophysical Journal*, **10:8**, pp. 773 – 796.

Forsberg, P.-O. (2010): "Identification and modeling of sensory feedback processing in a brain system for voluntary movement control." Master's Thesis ISRN LUTFD2/TFRT--5849--SE. Department of Automatic Control, Lund University, Sweden.

Fourcaud-Trocme, N., D. Hansel, C. van Vreeswijk, and N. Brunel (2003): "How spike generation mechanisms determine the neuronal response to fluctuating inputs." *Journal of Neuroscience*, **23:37**, pp. 11628–11640.

Fujita, M. (1982): "Adaptive filter model of the cerebellum." *Biological Cybernetics*, **45**, pp. 195–206. 10.1007/BF00336192.

Gomi, H. and M. Kawato (1990): "Learning control for a closed loop system using feedback-error-learning." In *Decision and Control, 1990., Proceedings of the 29th IEEE Conference on*, pp. 3289 –3294 vol.6.

Hebb, D. O. (1949): *The Organization of Behavior: A Neuropsychological Theory*, new edition edition. Wiley, New York.

Hille, B. (2001): *Ion Channels of Excitable Membranes*, 3rd edition edition. Sinauer Associates.

Hodgkin, A. L. and A. F. Huxley (1952): "A quantitative description of membrane current and its application to conduction and excitation in nerve." *The Journal of Physiology*, **117:4**, pp. 500–544.

Ito, M. (1984): *The Cerebellum and Neural Control.* Raven Press.

Ito, M. (2008): "Control of mental activities by internal models in the cerebellum." *Nature Reviews Neuroscience*, **9:4**, pp. 304–313.

Jörntell, H., F. Bengtsson, M. Schonewille, and C. I. De Zeeuw (2010): "Cerebellar molecular layer interneurons - computational properties and roles in learning." *Trends in Neurosciences*, **33:11**, pp. 524 – 532.

Jörntell, H. and C. Ekerot (2006): "Properties of somatosensory synaptic integration in cerebellar granule cells in vivo." *The Journal of Neuroscience*, **26:45**, pp. 11786–11797.

Jörntell, H. and C.-F. Ekerot (2002): "Reciprocal bidirectional plasticity of parallel fiber receptive fields in cerebellar purkinje cells and their afferent interneurons." *Neuron*, **34:5**, pp. 797 – 806.

Jörntell, H. and C.-F. Ekerot (2003): "Receptive field plasticity profoundly alters the cutaneous parallel fiber synaptic input to cerebellar interneurons in vivo." *The Journal of Neuroscience*, **23:29**, pp. 9620–9631.

Katayama, M. and M. Kawato (1993): "Virtual trajectory and stiffness ellipse during multijoint arm movement predicted by neural inverse models." *Biological Cybernetics*, **69**, pp. 353–362. 10.1007/BF01185407.

Kawato, M. (1999): "Internal models for motor control and trajectory planning." *Current Opinion in Neurobiology*, **9:6**, pp. 718 – 727.

Kawato, M. and H. Gomi (1992): "The cerebellum and vor/okr learning models." *Trends in Neurosciences*, **15:11**, pp. 445 – 453.

Kitazawa, S., T. Kimura, and P.-B. Yin (1998): "Cerebellar complex spikes encode both destinations and errors in arm movements." *Nature*, **392:6675**, pp. 494–497.

Koch, C. and I. Segev, Eds. (1998): *Methods in Neuronal Modeling: From Ions to Networks*, 2nd edition. MIT Press, Cambridge, MA, USA.

Koike, Y. and M. Kawato (1995): "Estimation of dynamic joint torques and trajectory formation from surface electromyography signals using a neural network model." *Biological Cybernetics*, **73**, pp. 291–300. 10.1007/BF00199465.

Manto, M. (2008): "The cerebellum, cerebellar disorders, and cerebellar research - two centuries of discoveries." *The Cerebellum*, **7**, pp. 505–516. 10.1007/s12311-008-0063-7.

Mapelli, J., D. Gandolfi, and E. D'Angelo (2010): "High-pass filtering and dynamic gain regulation enhance vertical bursts transmission along the mossy fiber pathway of cerebellum." *Frontiers in Cellular Neuroscience*, **5:0**, p. 12.

Palay, S. L. and V. Shan-Palay (1974): *Cerebellar cortex: cytology and organization*. Springer.

Purves, D., G. J. Augustine, D. Fitzpatrick, W. C. Hall, A.-S. LaMantia, J. O. McNamara, and S. M. Williams (2004): *Neuro Science*, 3rd edition edition. Sinauer Associates.

Saarinen, A., M.-L. Linne, and O. Yli-Harja (2008): "Stochastic differential equation model for cerebellar granule cell excitability." *PLoS Comput Biol*, **4:2**, p. e1000004.

Sarkisov, D. V. and S. S.-H. Wang (2008): "Order-dependent coincidence detection in cerebellar purkinje neurons at the inositol trisphosphate receptor." *The Journal of Neuroscience*, **28:1**, pp. 133–142.

Schweighofer, N., M. A. Arbib, and P. F. Dominey (1996): "A model of the cerebellum in adaptive control of saccadic gain." *Biological Cybernetics*, **75:1**, pp. 29–36.

Schweighofer, N., M. A. Arbib, and M. Kawato (1998): "Role of the cerebellum in reaching movements in humans. I. Distributed inverse dynamics control." *European Journal of Neuroscience*, **10**, pp. 86–94.

Schweighofer, N., K. Doya, H. Fukai, J. V. Chiron, T. Furukawa, and M. Kawato (2004): "Chaos may enhance information transmission in the inferior olive." *Proceedings of the National Academy of Sciences of the United States of America*, **101:13**, pp. 4655–4660.

Schweighofer, N., J. Spoelstra, M. A. Arbib, and M. Kawato (1998): "Role of the cerebellum in reaching movements in humans. II. A neural model of the intermediate cerebellum." *European Journal of Neuroscience*, **10:1**, pp. 95–105.

Smith, G. D., C. L. Cox, and J. Rinzel (2000): "Fourier analysis of sinusoidally driven thalamocortical relay neurons and a minimal integrate-and-fire-or-burst model." *Journal of Neurophysiology*, **83**, p. 588.

Sánchez, E., A. Reboreda, M. Romero, and J. Lamas (2006): "Spontaneous bursting and rhythmic activity in the cuneate nucleus of anaesthetized rats." *Neuroscience*, **141:1**, pp. 487 – 500.

Widrow, B. and E. Walach (2007): *Appendix G: Thirty Years of Adaptive Neural Networks: Perceptron, Madaline, and Backpropagation*, pp. 409–474. John Wiley & Sons, Inc.

Yamamoto, K., M. Kawato, S. Kotosaka, and S. Kitazawa (2007): "Encoding of movement dynamics by purkinje cell simple spike activity during fast arm movements under resistive and assistive force fields." *Journal of Neurophysiology*, **97:2**, pp. 1588–1599.